de Mesquita, Oscar Nassif

ASYMMETRY OF DYNAMICS AT THE GROWING CRYSTAL-MELT INTERFACE OF SALOL

City University of New York PH.D. 1984

ASYMMETRY OF DYNAMICS AT THE GROWING CRYSTAL-MELT INTERFACE OF SALOL

by

OSCAR NASSIF de MESQUITA

A dissertation submitted to the Graduate Faculty in Physics in partial fulfillment of the requirements for the degree of Doctor of Philosophy, The City University of New York.

1984

This manuscript has been read and accepted for the Graduate Faculty in Physics in satisfaction of the dissertation requirement for the degree of Doctor of Philosophy.

June 26, 1984
date

Chairman of Examining Committee

July 16, 1984
date

Executive Officer

Supervisory Committe

The City University of New York

Abstract

ASYMMETRY OF DYNAMICS AT THE GROWING
CRYSTAL-MELT INTERFACE OF SALOL

by

OSCAR NASSIF de MESQUITA

Adviser: Professor Herman Z. Cummins

Quasielastic laser light-scattering measurements on the b and a faces of a Salol crystal growing into the melt revealed simultaneous lateral translational dynamics on the crystal surface and slow relaxational dynamics in a thin boundary layer of melt adjacent to the crystal. The slow relaxational dynamics were also observed when the crystal was melting. Analysis of the translational dynamics shows that crystal growth is mediated by highly polygonized screw dislocations. Several mechanisms which can be considered to explain the boundary layer dynamics are discussed. However, a consistent physical model to explain the slow relaxational dynamics has not yet been achieved.

ACKNOWLEDGMENTS

I express my gratitude to Professor Herman Z. Cummins for his patient guidance and continued support during this thesis. I thank Dr. M.Copic for having initiated this experiment and built the first setup. I am specially indebted to Dr. Dennis Neal for his important contributions to the experiment during his tenure in this laboratory. I thank Professor J.H.Bilgram and Dr. P.Boni for several helpful discussions and for generously providing information and advice about sample preparation. I thank Dr. K.A.Jackson, Dr. W. van Saarlos, Dr. J.D.Weeks and Dr. G.H.Gilmer for very helpful discussions and for having provided reprints and preprints of their leading work in crystal growth. I thank all the members of the light scattering group, Dr. J.Wicksted, Dr. M.Matsushita, Dr. T.Shigenari, Dr. T.Aurora, Dr. M.Dutta, Mr. S.Qiu and Mr. X.Lu for their cooperation and for the pleasant working atmosphere. I thank Dr. M.Awal for advice in sample preparation and for having measured the indices of refraction of Salol. For their help and encouragement during these years, I and my family would like to thank Munemassa and Kyoko Machida, Juan and Olga Pajuelo, Helio and Barbara Grandinetti, Antonino and Carolina Rapazzo, Mike and Ruth DeMaio, and Sara Mendozza. We are very grateful to Mrs. Marsha Cummins for her support and encouragement in very difficult times, and to our neighbors Joe and Martha Winterholler our "step-parents" in this country. I acknowledge support from the government of Brazil through a CAPES fellowship, and the U.S. Department of Energy for having supported this research work under contract No. DE-AC02-79ER 10482.

DEDICATION

I dedicate this thesis to my parents, my wife Eda and my daughters Maira and Nara, for their love and comprehension during this work.

CONTENTS

I. INTRODUCTION

In this introduction a brief review of the major points of interest in, and of the historical background of the crystal-growth problem will be presented. Recent advances in the area of crystal growth will be briefly discussed. The references will be taken mainly from review articles in the field. A discussion of the traditional experimental methods in the study of crystal growth and the recent use of quasielastic laser light scattering technique to study dynamics at the growing crystal-melt interfaces, pioneered by Prof. J. H. Bilgram at the E. T. H. in Zurich, will also be presented. The topics which are more relevant to the understanding of the experimental results of this thesis are presented in separate chapters.

A. Interest in The Crystal-Growth Problem

Rapid expansion of the use of high-quality crystalline materials in electronic and optical devices during the past two decades has stimulated much research, both experimental and theoretical, on the dynamics of crystal growth. A better understanding of solidification processes in metals and the growth of eutectic fibers are also of unquestionable technological interest.

The surface of a growing crystal is not at equilibrium. As is now widely recognized, dynamical systems far from equilibrium exhibit novel instabilities often characterized by period-doubling bifurcations. The growing crystal interface can be viewed as a

nonequilibrium dynamical system and the interfacial dynamics studied as a function of the growth velocity v_G which plays the role of a bifurcation parameter.

It is generally recognized that a crystal can grow into the adjacent melt (or vapor or solution) by several different mechanisms, depending on the structure of the interface, purity, growth velocities, temperature gradients and related factors, and that the details of the growth mechanism strongly influence the quality of the resulting crystal.

For the crystal to grow it is necessary that,

(1) the atoms or molecules be transported to the interface where the phase transformation is taking place;

(2) the transported atoms or molecules must have nonzero probability of sticking on the interface;

(3) the latent heat generated in the growth process as well as the excess components segregated, must be conducted away from the interface.

(1) The transport of molecules to the interface in the case of vapor growth can be treated by the kinetic theory of gases. In the case of solution growth, diffusion of the solute in the liquid solvent is the mechanism of transport. In the case of melt growth, the mechanism of transport is not very clear since a closed packed liquid is adjacent to the interface. However, the experimental data for the melt growth of glass-forming materials has shown correlation between the transport process for crystal growth and the activated process for self-diffusion of the molecules in the melt[1]. Recent computer simulations on crystal growth from the

melt[2] have shown that an ordered stratified layer of melt develops ahead the interface of a growing crystal. Computer simulations on the equilibrium structure of crystal-melt interfaces indicate a very sharp transition (interface layer of one to two atomic distances) from solid to liquid[3]. Recent light scattering experiments at the crystal-melt interface of growing crystals[4-11], which will be discussed later in this thesis, indicate the presence of a boundary layer between the crystal surface and the bulk melt with physical properties different from the bulk melt properties, suggesting that the structure of the melt ahead of the crystal interface can be more complex than previously recognized.

(2) The sticking probability of molecules on the interface depends on the structure of the interface through the density of kink sites on the interface. The density of kink sites can be given in terms of the concentration of adsorbed atoms (adatoms) on the interface, also called adpopulation. (Note that we are using the terms atom or molecule loosely.) If the adpopulation is large ("rough" interface) the transported molecules will have a high probability of sticking on the interface whereas if the adpopulation is small ("smooth" interface) the probability of sticking will also be very small. The problem of calculating the adpopulation has been shown by Burton, Cabrera and Frank[12] to belong to a class of cooperative phenomena and exhibits an order-disorder type of phase transition, the roughening transition. The statistical mechanics of the roughening transition has been the subject of recent active research[13-15]. The roughening transition is of interest not only because of its implication for surface physics but also because of

the great interest in critical phenomena which has attracted the attention of condensed matter physicists to the problem.

(3) In the process of conduction of latent heat and excess material away from the interface, because of the competition between the interface energy (via capillary forces) and the heat and chemical fields, a morphological instability can occur. The planar interface may become cellular or dendritic. The first mathematical treatment of this morphological instability was done by Mullins and Sekerka in 1963 and 1964[16]. When the interface becomes unstable, a critical slowing down of the relaxation rate of the interface height fluctuations is predicted to occur. This phenomenon has never been observed experimentally, mainly because the traditional experimental techniques used in crystal growth could not probe the dynamics of the interface in a microscopic scale. Efforts have been made in our laboratory to detect this instability with the use of light scattering techniques to be discussed later.

The nonequilibrium and nonlinear features of this problem has recently also attracted the attention of theoretical physicists, whose contribuitions in the field have been very profitable[17,18]. The most complete measurements for dendritic growth was performed recently by Glicksman et al.[19] in succinonitrile. This morphological instability in crystal growth is one of the most elegant examples of pattern selection and self-organization in nature. The theory has been recently reviewed by Langer[17].

B. Historical Review of the Theory of Crystal Growth

1) Early Theories

The first theory of crystal growth was proposed by H. Wilson[1] in 1900 and independently by J. Frenkel[20] in 1932. In the Wilson-Frenkel theory all the sites on the interface were assumed to be active growth sites, so the structure of the interface was not taken into account. This theory may be applied to crystals with microscopically "rough" interfaces but not for crystals with "smooth" interfaces[13]. The growth occurs by the vertical piling up of the atoms on the interface. The mechanism is called continuous since there is no resistance to the sticking of atoms on the interface, therefore very small driving forces result in growth. The growth rates derived in this theory are an upper limit for actual growth rates. The most striking experimental evidence for the validity of the Wilson-Frenkel theory for "rough" surfaces is provided by growth rate experiments in GeO_2[21].

Volmer and subsequently Becker and Doring[14] proposed a nucleation theory for crystal growth, which can be applied for "smooth" interfaces[13]. In this theory a small cluster of atoms is nucleated on the "smooth" interface, and the growth proceeds by the lateral spreading of the layer then initiated. However, the nucleation theory predicts negligible growth rates at small undersaturations (undersaturation being the difference in chemical potential between the two phases), whereas in practice much higher growth rates were observed. This discrepancy led Frank[22] to suggest the importance of crystal defects in crystal growth. In particular, he suggested that the presence of screw dislocations would provide

perpetual growth steps on the crystal surface, the nucleation of clusters then being unnecessary for growth to progress. Both nucleation and screw dislocation mechanisms are called lateral mechanisms since the growth occurs by the lateral spreading of layers. Besides the indirect evidence for the screw dislocation growth mechanism obtained from growth rate measurements, direct evidence of "Frank spirals" can be obtained by observing the faces of crystals with microscopy techniques. The first observation of these spirals was reported by Griffin[23] on a natural beryl crystal. Soon after that several observations were made in crystals grown from the vapor, which were summarized by Verma[24]. The first observation of growth spirals in solution-grown crystals was reported by Forty[25], and the first observation of growth spirals in melt-grown crystals was reported by Sears[26]. An excellent review of the theory and the most recent experimental techniques and observations of growth spirals can be found in the review article by Sunagawa and Bennema[27]. It is interesting to note that most of the recent advances in the study of spiral growth have occurred in connection with Geological studies. From the analysis of the morphology of the growth spirals in natural materials, the approximate conditions of temperature and pressure when the geological formations occurred can be inferred. Recently the growth and dissolution of Frank spirals were also observed in the growth and melting of liquid-crystals in their "blue phases"[28].

The early theories of crystal growth will be discussed in more detail in chapter II of this thesis.

2) Burton, Cabrera and Frank Theory

We could say that the Burton, Cabrera and Frank[12] theory of crystal growth published in 1951, the BCF theory, was the first more or less complete theory of crystal growth, since the growth kinetics as well as the structure of the interface were discussed. The theory was mainly concerned with growth from the vapor. In their study of spiral growth, they demonstrated that after few turns the spiral becomes almost an ideal Archemedian spiral. By knowing the distance between the arms of the spiral, the number of growth sites could be calculated and consequently the kinetics of the growth could be determined. They were the first in recognizing and treating the interface structure problem as a cooperative phenomenon exhibiting an order-disorder phase transition: the roughening transition. Above the roughening temperature the crystal surface would be "rough", and below the roughening temperature the crystal surface would be "smooth". They used the Ising model to calculate the adpopulation on the interface. Two-level and multilevel models of the interface were treated, but for all of them the roughening temperatures for the lowest index faces were found to be above the melting temperature. Then, erroneously, they concluded that the roughening transition would not be important for crystal growth.

3) Jackson's Theory

Jackson[13] in 1958 proposed a theory for the structure of the interface which is remarkably successful in its predictions. The statistical model used in the calculation was a two-level Bragg-

Williams model, where the important parameter used to calculate the adpopulation on the interface was the latent heat of the transformation rather than the binding energy used in the BCF theory. Thus, for melt-growth where the latent heat for some materials is relatively small, the adpopulation can be very large leading to "rough" low index interfaces on an atomic scale[29]. Jackson, rather than dealing with the roughening temperature, introduced the parameter α as a criterion to determine if a particular crystal growing from a particular phase would display "rough" or "smooth" interfaces. (α will be defined in Chapter II). His criterion is fully suported by experimental observations, and we cite two experiments where the roughening transition was observed: the work by Jackson and Miller[30], where the roughening transition was observed in vapor-growth of C_2Cl_6 and NH_4Cl crystals, and the work by Avron et al.[31] where the transition was observed in the melt-growth of ^4He.

Jackson's theory will be further discussed in Chapter II of this thesis.

4) Cahn's Theory of The Diffuse Interface

Because the grain boundary energy was observed to be larger than twice the interfacial energy between the solid and its melt (for the case of gold, copper and silver), Hilliard and Cahn[32] concluded that the interface in such systems is diffuse. From the assumption of a diffuse interface between the crystal and its melt, Cahn, Hillig and Sears[33] proposed a new theory for the structure of the interface. The main consequence of their theory is

that at sufficiently small undercoolings all crystals would grow by a lateral mechanism (nucleation or screw dislocation mechanisms), whereas above a certain critical undercooling the mechanism would be continuous (Wilson-Frenkel mechanism). This transition became known in the literature as lateral-to-continuous transition in crystal growth. Although Jackson's theory predicts a "kinetic roughening" in "smooth" interfaces at large undercoolings, the interfaces which are already "rough" at equilibrium, no matter how small the undercooling, would always grow by a continuous mechanism, in direct contradiction with Cahn's theory. Since the diffuseness of the interface cannot be calculated from first principles, Cahn used a phenomenological description of the structure of the interface. The transition temperature is obtained by fitting the theory to the kinetic data.

Jackson, Uhlmann and Hunt[34] have shown that Cahn's theory as derived could be applied to systems which can have a second order phase transformation, but not to liquid-solid or vapor-solid phase transformations which are first order. They modified Cahn's theory to be applicable to first order phase transformations, but reasonable agreement with experiment still could not be obtained. Jackson et al. made a careful analysis of the experimental data used by Cahn et al. in support of their theory, showing that most of the quantitative data on crystal growth available were of questionable reliability or were not sufficiently complete for detailed comparison with theory[34].

5) Recent Advances in the Roughening Transition Problem

Most of the results stated in this section (as well as the references) were taken from the review articles by Jackson[14], and by Weeks and Gilmer[15].

a) statistical models

In several studies of the equilibrium properties of the interface structure, the Ising model was used. Only the one-dimensional and two-dimensional Ising models have been solved exactly. The three-dimensional model, in a homogeneous phase, has not been solved exactly. Consequently, the surface of a three-dimensional Ising model has not yet been solved exactly. Several approximations have been used in an attempt to clarify the interface structure problem. However, only the very simplest models can be solved analytically. Jackson's model is a two-dimensional model and the Bragg-Williams approximation was used. This model exhibits a surface roughening transition for temperatures below the melting temperature. Three-dimensional models of the interface have also been studied and the simplest of these, the mean field model used by Leamy and Jackson (1971), does not exhibit a roughening transition. The same is true for the Bethe approximation used by Gilmer, Leamy, Jackson and Reiss (1974). However, low temperature expansion results by Weeks, Gilmer and Leamy (1973), the gaussian model by Weeks and Chui (1976) and the six vertex model by Van Beijeren (1977) all show a singularity indicating the presence of a roughening transition.

b) computer simulations

Computer simulations by Leamy and Gilmer (1974) and by Leamy, Gilmer and Jackson (1975) exhibit roughening transitions. In particular, the simulation by Leamy and Gilmer shows the step free energy going to zero as the roughening temperature is approached. This very interesting result indicates that the nucleation barrier for crystal growth goes to zero at the roughening temperature. Therefore the nucleation mechanism of growth can be operative at much smaller undersaturations than those predicted by the classical nucleation theory. The expression for the growth rate derived in the classical nucleation theory is still valid, provided that the correct value for the step free energy is used, not the bulk value traditionally employed. Therefore, the early theories of crystal growth are extremum cases, the continuous mechanism being valid above the roughening temperature and the lateral mechanisms being valid well below the roughening temperature.

6) Modern Theory of Spiral Growth

For a review of the theory and experiments on spiral growth we again suggest the review article by Sunagawa and Bennema[27]. The references cited here were taken from this review article.

The modern theory of spiral growth concerns the analysis of the kinetics and morphology of growth spirals originating at screw dislocations, within the context of the interface structure problem. Thus, again, the Jackson α-factor is the parameter which determines the important properties of the spiral. Whether a spiral takes a circular or polygonal form is mainly controlled by the roughness of the spiral step. If the step is rough, i.e., the kink

density is high, the step can advance independently of crystallographic directions, and the spiral becomes round. If the step is smooth, i.e., the kink density is low, the crystallographic directions show up more and the spiral becomes more polygonized. Therefore, as the Jackson α-factor increases, the polygonization also increases.

Computer calculations by Muller-Krumbhaar, Burkhardt and Kroll (1977) indicate that the distance between arms of a round spiral becomes smaller as the spiral becomes more polygonized. They showed analytically that if the anisotropy of the step free energy is the same as the diffusion fields, the evolution of the spiral is shape-preserving, the spiral having the same shape as the critical nucleus for layer nucleation. Further, Muller-Krumbhaar et al. showed that the round to polygonized transition far from the center of the spiral occurs for $\alpha \sim 7$ and polygonization in the center for $\alpha \sim 25$. They neglected surface diffusion in the calculation as well as the more complex structure of real materials, which would decrease the value of α for these transitions.

As in the case of the interface structure problem, very few examples can be worked out analytically. Again the computer simulation results become very important. Spiral growth has been simulated by Gilmer and Bennema (1972) and by Gilmer (1976).

C. Experimental Techniques

Experiments in crystal growth from the melt (solidification) have provided most of the data for the understanding of the crystal growth processes. The Wilson-Frenkel theory was originally

applied to solidification. In this discussion of experimental techniques we restrict ourselves to the discussion of experimental methods in crystal growth from the melt.

1) Kinetic Studies

For this section see the review article by Jackson, Uhlmann and Hunt[34].

By kinetic studies we mean the analysis of the functional relationship between growth velocity and the undercooling of the interface. This functional dependence between growth velocity and undercooling is different for each mechanism of growth. Therefore, in principle, the mechanism of growth can be determined from the kinetic data. However, there are experimental problems in determining the temperature of the interface. In many experimental situations, growth is controlled by heat-flow rather than by the interface; that is, the growth rate is limited not by interface kinetics, but by the rate at which the latent heat of solidification generated in the growth process can be removed from the solidification front. In these cases the interface undercooling, for measurable growth rates, can be a small fraction of other temperature differences present in the system. Several techniques have been used in attempting to solve this problem.

(a) growth in capillary tubes

Capillary tubes are used to minimize the amount of latent heat generated at the interface. Even in this case, the growth must be slow enough so that the latent heat can be rapidly conducted away from the interface by the temperature gradients present in the system. Under these circumstances we could consider

the interface temperature as being equal the external bath temperature. However, there is no direct way of predicting when this approximation breaks down. Also, the effects of the substrate (capillary tube) on the growth rate may represent another source of problems.

(b) stirred melt

Stirring the melt increases the rate of dissipation of the latent heat by convection. The growth rate initially increases with stirring rate until it levels off. In this situation, in principle, the latent heat is no longer limiting the growth, thus the pure interface kinetics can be determined. However, it is common in this technique that nucleation starts to occur in the melt as the stirring speed and undercooling are increased, limiting the range of undercoolings available[35]. Also the stirred melt adjacent to the interface can cause unpredictable effects on the growth rate.

(c) theoretical treatment of heat flow

Under some circumstances, when the detailed heat flow in the apparatus is known, a theoretical treatment yielding corrections to obtain the temperature of the interface may be tried. Such treatments are likely to introduce other errors in the results. This is the approach used by us to determine the temperature of the interface in our experiment.

(d) Thermal wave technique

In this approach, a solid-liquid interface is located in a fixed temperature gradient, and an additional heat flux which in principle varies sinusoidally with time is introduced into the liquid. This causes the interface to move back and forth and hence

acts as a sink (in melting) or source (in freezing) of heat. This latent heat wave will be out of phase with the incoming thermal wave. By measuring the amplitudes and phases of the thermal waves with thermocouples located on both sides of the interface, it is in principle possible to calculate both the growth rate and the interface undercooling. In practice, however, its usefulness has been limited by experimental problems such as convective motion in the liquid, insufficient sensitivity of thermocouples, and nonsinusoidal thermal waves. Further, a complex theoretical analysis must be employed to obtain the relation between growth velocity and undercooling from the experimental data. This technique was used by Kramer and Tiller (1965) and by Rigney and Blakely (1966) in tin. The two investigations gave widely different results.

(e) materials of high viscosity

The study of the growth of glass-forming materials which have high viscosity at their melting point can circumvent problems associated with the latent heat. In such cases the growth velocity, and therefore the generation of latent heat, is slow even at high undercoolings. That is the case of Salol, the organic crystal studied in this thesis. However, in this case a very accurate determination of the viscosity is required.

(f) reliability of kinetic data

Cahn et al.[33] used the kinetic data for Salol as one of the most important pieces of experimental evidence for their theory. The break in the kinetic curve would be evidence of the lateral-to-continuous transition. However, Jackson et al.[34] have repeated

the kinetic measurements in Salol and they showed that breaks in kinetic curves can occur for different reasons such as a change in morphology of the growing crystal, and that the presence of dissolved gases and impurities can strogly affect the measurements. They emphasized the importance of morphological studies being performed simultaneously with kinetic studies to determine the mechanism of growth.

An extensive review on the kinetics of crystal-growth from the melt for various materials can be found in the review article by Ovsienko and Alfintsev[36]. The predictions of Jackson's and Cahn's theories are discussed and compared with experimental data.

2) Morphlogical Studies

The morphology of interfaces can be studied most directly by microscopy techniques. The first observations of growth spirals were done with ordinary optical microscopes. In this case only spirals with very large step heights (more than 1000Å) could be observed. Monomolecular spirals, i.e., spirals with a step height of one lattice spacing, can be observed with ordinary optical microscopes when heavily decorated by foreign materials[27]. However, no quantitative information about the step height can be obtained. Phase contrast microscopy permits the observations of spirals with step heights of less than 10Å. However, the most sensitive and precise method to measure very small step heights is the multiple-beam interferometry technique developed by Tolansky[37].

The smallest step height of a spiral so far reported is 2.3Å, corresponding to a layer with the smallest possible height in the structure of Fe_2O_3, which was observed and measured by Sunagawa[27]

on natural hematite.

Electron-microscopy has also been used with success in some materials. As a reference we cite the interesting article about growth and dissolution of spirals by Kaganovskii and Onoprienko[38]. However all these techniques only give static information about the interface.

3) Simultaneous Kinetic and Morphological Studies

The only in situ direct observation of spiral growth so far reported is the work by Tsukamoto[39]. By combining optical phase contrast microscopy with a conventional TV system, monomolecular spiral growth steps on crystals were observed during growth in aqueous solution. Therefore, morphological information about the spiral as well as the lateral velocity of the growth steps could be obtained as a function of undersaturation.

In this thesis we will show that simultaneous morphological and kinetic information on growth spirals can be obtained with laser light scattering techniques used in situ at the interface of a Salol crystal growing from the melt.

D. Quasielastic Laser Light Scattering

The development of ultrahigh resolution laser light scattering techniques in the 1960s provided a new experimental approach to exploring dynamical phenomena in the kilohertz frequency range which proved to be ideally suited for the study of low frequency excitations in a wide range of physical systems.

1) Brief Historical Background

The phenomenon of light beating was first demonstrated in the classic experiment of Forrester, Gudmundsen and Johnson[40] in 1955. The 5461Å Zeeman-split light from a ^{202}Hg lamp was incident on a photomultiplier tube. The beating of the two components of the light in the photomultiplier produced an a.c. component in the output photocurrent at the Zeeman difference frequency. Although this experiment clearly demonstrated the light-beating phenomenon, the measurement was extremely difficult primarily because of the low intensity and large linewidth of the light source. A dramatic change occurred with the advent of lasers, the light beating phenomenon becoming easily observable, and becoming a standard technique in laser laboratories. The possibility of using the light-beating phenomenon as a spectroscopic technique was demonstrated theoretically by Forrester[41] in his 1961 paper "Photoelectric Mixing as a Spectroscopic Tool". Since then, Photon Correlation Spectroscopy, or Light Beating Spectroscopy, or Quasielastic Light Scattering Spectroscopy has been applied in the study of a very large number of physical systems. For review of the theory and experiments in this field we refer to Cummins and Swinney[42] and Cummins and Pike[43].

One of the first works in Doppler-Velocimetry using Photon Correlation Spectroscopy was done by Cummins et al.[44] in 1963. In this experiment a traveling ultrasonic wave is produced in the bulk of water placed in a container. The incident laser light is Bragg diffracted and Doppler shifted by the traveling ultrasonic water wave. The beating of the diffracted light with part of the

incident beam occurs in the photomultiplier tube (heterodyne detection). The frequency of the a.c. component of the output photocurrent is related to the velocity of the traveling ultrasonic water wave by the well known Doppler-shift equation. This experiment closely resembles the experiment that will be described in this thesis. We will show that the motion of the legdes of polygonized screw dislocations, which are responsible for the growth in this case of Salol grown from the melt, Bragg diffracts and Doppler shifts the light.

2) Photon Correlation Spectroscopy and Dynamics at the Growing Crystal-Melt Interface

The first experiment using Photon Correlation Spectroscopy to study dynamics at a growing crystal-melt interface was reported in 1978 by Bilgram, Guttinger and Kanzig[4,5], on the growing ice-water interface. The relaxational intensity autocorrelation function observed in this experiment was interpreted as being caused by time dependent surface roughness fluctuations. Subsequently, Boni and Bilgram[6,7] have shown that the scattered light was caused by fluctuations in a boundary layer between the crystal surface and the bulk melt. They interpreted their data in terms of an anomaly in the heat diffusion mode. To find out if this anomalous scattering was a property only of the ice-water interface, Durig and Bilgram[8] performed experiments on the growing crystal-melt interface of Salol. In this experiment, besides a relaxational intensity autocorrelation function similar to that observed at the ice-water interface, they also observed an oscillatory one. They interpreted

the oscillatory scattering as being caused by the lateral motion of growth steps on the crystal surface, which Doppler shift the light. In a recent article[11] we demonstrated that the steps moving laterally on the interface are the ledges of polygonized spirals originated at screw dislocations. Recently Durig[9] has given a similar interpretation to the moving steps on the interface.

Yeh and co-workers[10] have also done experiments at the ice-water interface obtaining results similar to those of Bilgram's group.

3) Our Salol Experiment

Salol is one of the "favorite" materials for crystal growth studies, because:

- it has a convenient melting temperature, about 41°C;
- it is transparent to visible light;
- its growth is slow at reasonable undercoolings, making Salol very suitable for interface kinetics studies;
- a large amount of information about Salol is available in the literature.

In addition, we chose Salol because of the interesting preliminary results obtained by Durig and Bilgram[8] which, at that time, had not been described by a physical model.

In our Salol experiment we showed that the relaxational and oscillatory scattering occur simultaneously: the oscillatory scattering occurring at the crystal surface and the relaxational scattering occurring in a thin boundary layer between the crystal surface and the bulk melt. For the first time the relaxational

scattering was also observed when the crystal was melting. The relaxational scattering observed when the crystal is growing or melting are similar, and the only noticeable difference is the minimum velocity for the onset of the scattering, which is ~0.04 μm/s when growing and ~0.5 μm/s when melting.

We demonstrated that the oscillatory scattering is caused by the motion of the ledges of polygonized spirals originating at screw dislocations. The quasiregular distance between the arms of the spiral is of the order of the wavelenght of the incident light, causing Bragg diffraction of the light and giving as a result a very anisotropic scattering. The motion of the steps Doppler shifts the light. Beating of the Bragg diffracted (and Doppler shifted) light with elastic scattered light in the photomultiplier produces the characteristic oscillatory correlation function. From the frequency of the oscillation, the lateral velocity of the steps on the interface could be obtained. From a computer fit of lateral velocity versus the normal growth velocity, the growth mechanism was determined without reference to the undercooling of the interface. Further, from an independent analysis of the vertical temperature profile, we could obtain the kinetic coefficient of the growth using two different approaches. The resulting values are self-consistent and in agreement with known literature values. The morphology of the spirals was also obtained from the measurements.

A discussion of several mechanisms that can be considered to explain the relaxational scattering is presented. However, a consistent physical model for this problem has not yet been achieved.

II. THEORY OF CRYSTAL GROWTH FROM THE MELT

An excellent introduction to the theory of crystal growth from the melt can be found in the book "The Solid-Liquid Interface" by D. P. Woodruff[45]. Various theories of crystal growth mechanisms have been proposed since 1900, and are still in the process of development and revision[14,15,45,46]. The principal theories can be roughly divided into four categories.

A. Wilson-Frenkel model - continuous growth

The first theory of crystal growth was proposed by H. A. Wilson in 1900[1] and independently by J. Frenkel in 1932[20]. The basic assumption of the model is that the crystal growth is a reversible process in which atoms are both leaving and joining the crystal. It is also assumed that both the rate of arrival of atoms and the rate of departure can be calculated assuming simple activated processes. The model does not take into account the structure of the interface, since it assumes that all the sites on the interface are active growth sites. We shall see later that this last assumption is valid only for a class of materials for which the interface is microscopically "rough"[13]. The activated process for arrival of atoms was associated with the temperature dependence of the viscosity of the liquid phase. Thus the model predicts a growth velocity proportional to the undercooling of the interface for small undercoolings, the undercooling being the difference between the melting temperature T_m and the actual temperature of the interface T_i, and inversely proportional to the viscosity of the fluid phase. There is no barrier to be overcome by the growth

front, the crystal growing normal to itself rather than by the spreading of layers. For this reason this growth mechanism is called "continuous". The growth is controlled by diffusion of heat and mass. The interface takes the shape of an isotherm of the system. For small undercoolings, i.e., $L\Delta T/kT_mT_i<<1$, where L is the latent heat of fusion, ΔT is the undercooling of the interface, k is the Boltzman constant, T_m is the melting temperature and T_i is the actual temperature of the interface, the resulting kinetic equation can be written as:

$$v_G = \mu_1 \Delta T \qquad 2.1$$

where v_G is the growth velocity, ΔT is again the undercooling, and μ_1 is the kinetic coefficient derived in the Wilson-Frenkel theory:

$$\mu_1 = D \frac{\Delta S}{a\ k\ T_i}$$

where D is a diffusion coefficient related to the transport of molecules from the melt to the crystal surface assumed to be equal the self-diffusion coefficient of the bulk melt phase, ΔS is the melting entropy, a is the jump distance for diffusion, and k and T_i have the same meanings as before. The coefficient D has the same temperature dependence as the bulk melt self-diffusion coefficient, however if the value of the self-diffusion coefficient in the bulk melt is used to calculate the kinetic coefficient μ_1, the result is two to three orders of magnitude smaller than the

experimental value obtained from kinetic data. It indicates that the transport of molecules at the interface which is important for crystal growth is much slower than that in the bulk melt. For crystals with faceted morphologies, the growth velocity versus undercooling behaviour was observed to have different functional forms than linear. Therefore, other growth mechanisms were proposed.

B. Nucleated Layer Growth

For crystals with faceted morphologies ("smooth" interfaces)[13], an important mechanism for growth is that of layer growth mediated by surface nucleation. In this theory a layer one molecule thick is nucleated when a small cluster of molecules having a radius larger than the critical radius for two-dimensional nucleation sticks to the surface, and the new layer then spreads out across the surface until the layer is completed. The first nucleation theory of growth was proposed by M. Volmer in 1934 and subsequently put on a more firm basis by R. Becker and W. Doring in 1935[14]. The nucleation theory leads to an exponential dependence of the growth rate on undercooling. In the derivation of the kinetic equation for the nucleation mechanism, Jackson[47] multiplied the growth rate given by the Wilson-Frenkel model by the number of growth sites on the interface derived from the nucleation theory. Besides the exponential dependence on undercooling, he obtained a prefactor which is linear in undercooling. However, the growth rate is very insensitive to this prefactor allowing us to write the kinetic equation as:

$$v_G = \mu_2 \exp(-\frac{K}{\Delta T}) \qquad 2.2$$

where K is a constant which involves the step free energy of the cluster of molecules.

At low undercoolings, the predicted rates turn out to be vanishingly small, whereas in practice much larger rates are observed. The importance of defects as growth sites on the interface of crystals therefore must be considered.

C. Screw Dislocation Growth

At very small undercoolings an important growth mechanism for faceted crystals is screw dislocation mediated growth, proposed by F. C. Frank[22] in 1949. Screw dislocations provide a mechanism for layer growth without requiring surface nucleation. Once a screw dislocation appears on the crystal surface, the ledge will wind around the screw axis in the form of a faceted spiral, providing continuous sites for layer growth without requiring continuous layer nucleation. Each layer spreads across the crystal surface until it reaches either a rigid boundary or another dislocation. The kinetic equation for this mechanism in the case of melt growth was derived by Hillig and Turnbull[48] and can be written as:

$$v_G = \mu_3(\Delta T)^2 \qquad 2.3$$

where v_G is the growth velocity, ΔT is the undercooling and μ_3 is the kinetic coefficient for screw dislocation growth. μ_3 can be

written as:

$$\mu_3 = \frac{3(\Delta S)^2 D}{s\ a\ k\ T_i\ \sigma}$$

where ΔS, D, k, and T_i have the same meanings as before, σ is the step free energy, and s is the parameter of the spiral, which is 19 for round spirals and 5.4 for polygonized spirals[27]. The factors 19 or 5.4 are the parameters if only one spiral is responsible for the growth. However, in practice that is not usually the case and a great number of screw dislocations may exist simultaneously during the growth process. The interaction between screw dislocations can be complex, giving rise to several different patterns[27]. However, generally we could say that the presence of more than one screw dislocation on the interface makes the parameter s decrease as compared with the ideal situation of a single spiral covering the whole interface. Experiments by Kirtsinghe (reviwed by Strickland-Constable[46]) showed that when the growing face of a Salol crystal growing into an undercooled melt entered a glass capillary, the growth rate decreased almost to zero for fixed undercooling. The freely-growing crystal exhibited an etch pit density of $\sim 10^5$ cm^{-2}, while sections from regions of slowest growth exhibited $\sim 2 \times 10^2$ cm^{-2}. The etch pits presumably occured at the centers of screw dislocations, confirming the dependence of μ_3 on the density of screw dislocations.

Most of the evidence for screw dislocations is static, obtained by optical or electron microscopy[27] of crystal surfaces exhibiting

such spirals, or from the observation of etch pits presumed to occur at dislocation sites. Recently, Tsukamoto[39] by combining optical phase contrast microscopy and a conventional TV system, observed spirals growing from aqueous solution directly in situ. In the experiment described in this thesis, light scattering studies of the crystal-melt interface of Salol (phenyl salicylate, $C_{13}H_{10}O_3$), revealed the growth dynamics of screw dislocations indirectly.

D. Dendritic Growth and the Mullins-Sekerka Instability

At high growth rates the planar interface of crystals exhibit dynamic height fluctuations about the mean interfacial plane. Because fluctuations induce local curvature of the interface, they introduce restoring forces which make them decay. Thus the nonequilibrium interface exhibits relaxing fluctuations in height similar to overdamped capillary waves on the equilibrium surface of a viscous fluid. These waves are not thermally excited, however. They are driven by the kinetics of the crystallization process.

As the growth velocity into an undercooled melt increases, these interface fluctuations are expected to slow down and eventually become unstable. This morphological instability was first discussed by Mullins and Sekerka[16] and has been thoroughly reviewed by Langer[17]. The underlying physical origin of this dynamical instability for pure systems is the production and dissipation of latent heat of fusion liberated by the advancing crystal front. If the melt is undercooled, an inverted temperature gradient develops ahead of the interface which steepens with increasing growth rate.

When a "bump" appears on the interface, it extends through part of the warmer layer into the cooler melt. Since greater undercooling implies greater growth rate, the inverted temperature gradient tends to amplify the bump in direct competition with the excess energy of curvature which causes it to decay. At a critical growth velocity v_c the two forces just balance, and the relaxation rate reaches zero (for a particular critical wave-vector q_c). For growth velocities greater than v_c the planar interface is unstable and will spontaneously develop protruding dendrites.

The spatial pattern which develop in the crystal-melt interface once this morphological instability has occurred can be complex and are the subject of considerable current research[17,18].

E. Jackson's Theory of the Solid-Liquid Interface

We have previously introduced the concepts of "rough" and "smooth" interfaces in connection with the morphology of non-faceting and faceting crystals, as well as in connection with the different kinetic laws obtained for the growth of these crystals. A remarkably successful theory about the structure of the interface was proposed by K.A.Jackson in 1958[13]. This theory predicts that close to thermodynamic equilibrium, solids in contact with their melts (or vapor) having the parameter $\alpha=\xi L/kT_E$ smaller than 2, will have "rough" interfaces, whereas for α greater than 2 they will have "smooth" interfaces, on an atomic scale. ξ is the number of nearest-neighbor sites in a layer parallel to the surface, divided by the total number of nearest-neighbor sites. L/kT_E is the ratio of the binding energy at the interface (taking into account

the other phase) to the thermal energy. L is the latent heat of fusion for a solid-liquid interface and the heat of vaporization for a solid-vapor interface.

Most metals in contact with their melts have $\alpha<2$ and they grow by a continuous mechanism showing no faceted morphologies. However, metals growing from the vapor phase display faceted morphologies and in fact, in this case they have $\alpha>>2$, typically about 10 to 20. Most organic crystals, Salol being a typical example, have high Jackson α-factors when growing from their melts. They display very strongly faceted morphologies and the mechanisms for growth are lateral, namely surface nucleation and screw dislocation growth. From Jackson's theory it was possible to predict which transparent materials would solidify like metals[49], improving considerably the understanding about the solidification processes in metals.

Most materials when growing from the melt are always either above or below their roughening temperatures (α smaller than 2 or larger than 2). To observe the roughening transition for the melt-growth case it is necessary to vary α by varying the melting temperature of the material. Only enormeous pressures can significantly change the melting temperature of most materials, making the transition experimentally inaccessible. Therefore, the crystal-vapor system is more convenient for observing the roughening transition, since the equilibrium temperature (and α) can be varied continuously by varying the vapor pressure of the system. The first experimental observation of the roughening transition was reported by Jackson and Miller[30] for the vapor-growth of C_2Cl_6 and

NH_4Cl. The roughening transition was also observed for the melt-growth of ^4He by Avron et al.[31]. The melting entropy of ^4He tends to zero for temperatures close to zero degree Kelvin. In a very small range of low temperatures the melting entropy of ^4He can be varied by several orders of magnitude, and therefore the Jackson α-factor in this system can be also varied continuously from values larger than 2 to values smaller than 2. The transition was detected by observing the loss of facets in the ^4He crystals.

III. Previous Light Scattering Experiments at the Solid-Melt Interface of Growing Crystals

A. Ice-water interface experiments

1)experiment performed by J.H.Bilgram, H.Guttinger, and W.Kanzig[4,5]

The first quasielastic light scattering investigations of the growing crystal-melt interface was reported in 1978 by J.H.Bilgram, H.Guttinger, and W.Kanzig. In their experiment, (performed at the E.T.H.,Zurich) a small ice crystal was placed in a growth tube containing highly purified water and gradually lowered through a zone-refining apparatus. A 4880 $\mathring{A}$ argon ion laser beam was focused onto the crystal-melt interface of the growing ice crystal from the water side, and light scattered at selected angles away from the reflected beam was directed to a photomultiplier. Analysis of the time averaged photocurrent and the photocurrent autocorrelation function gave the intensity and spectrum of surface fluctuations at the wavevector **q** selected by the scattering geometry. The principal results of this experiment were :

1) scattering was only observed if the critical growth velocity 1.5 $\mu m\ s^{-1}$ was exceeded;

2) after the scattering had been established, it was also observed if the growth velocity was decreased below the critical velocity, only disapearing if the surface was melted back (hysteresis) ;

3) the scattering was never observed during melting, but they noted that realizable melting velocities were considerably below the critical velocity;

4) the autocorrelation function of the scattered intensity was a single exponential and the linewidth Γ was found to be proportional to the square of the scattering vector. It is important to mention that their geometry only allowed them to perform the experiment with the scattering vector nearly parallel to the interface plane. The value found was $\Gamma = 4 \times 10^{-8} q^2\ s^{-1}$, for crystals growing along the c-axis ;

5) Γ was found to be independent of the growth velocity;

6) the width of the scattering region was estimated to have an upper limit of 6 μm from measurements of the spatial coherence properties of the scattered light;

7) the scattered light was also observed at the interface of crystals growing along the a-axis.

They initially interpreted their data as scattering from fluctuating random surface corrugations of the interface, relative to the mean interface level. They used the Gibbs-Thomson equation to calculate the local change in melting temperature caused by the curvature of the interface. This model predicted the value $\Gamma = 3.8 \times 10^{-8} q^2\ s^{-1}$ in excellent agreement with the experimental value.

2) experiment performed by P.Boni, J.H.Bilgram, and W.Kanzig[6,7]

The first results from this experiment were reported in 1980 and completed in 1983. Their apparatus is essentially the same as

that used in 1). The results refer to ice crystals growing along the c axis. The main results were :

1) the linewidth Γ is proportional to the square of the total scattering vector ($\Gamma = Dq^2$) , rather than being proportional to the square of the projection of the scattering vector on the interface;

2) the scattering is taking place not at the crystal surface but in a thin boundary layer between the crystal surface and the melt;

3) by using a scattering geometry such that the scattering vector has a minimum accessible length and is normal to the interface, they probed Fourier components of the fluctuations with wavelengths as large as 1.4 μm. Since the same "diffusion coefficient" D was obtained, they interpreted this length as a lower limit for the thickness d of the layer with the argument that the dynamics of the Fourier components in the layer can be only isotropic if their wavelengths are small compared to d.

4) Γ is independent of growth velocity;

5) the critical growth velocity for the onset of scattering was found to be proportional to the temperature gradient in the ice G_i. In the interval $2<G_i<4.5$ K cm^{-1}, the proportionality factor is $6.0\times10^{-5} cm^2 s^{-1} K^{-1}$;

6) there is a transient period where both linewidth and intensity vary, and are related by the equation

$$\Gamma = f(I)^{-\alpha}$$

where $\alpha=0.230\pm0.002$, $f=2750\pm27$ rad s^{-1} and I is the intensity in units of 1000 counts/s. The parameters α and f were found to be dependent on the temperature gradient, f being considerably larger

for larger G_i, indicating that the lifetime of the fluctuations is shorter at higher temperature gradients.

They interpreted the data on the basis of an anomaly in the thermal diffusion mode. From this conjecture and from Brillouin light scattering data, they concluded that the isothermal compressibility of this boundary layer is 700 times larger than that of the pure water, while the adiabatic compressibility was about the same as in pure water.

3) experiment performed by R.A.Brown, J.Keizer, U.Striger, and Y.Yeh[10]

The experiment was performed at the ice-water interface of crystals growing along the a axis. The main results were :

1) the critical growth velocity for the onset of the scattering was found to be about 0.5 μm s^{-1}. In particular, for this growth velocity of 0.5 μm s^{-1} the time for the onset of scattering was about 60 minutes after the interface had reached the stationary position. For higher growth rates the time for the onset of the scattering was found to be about the same as the time for reaching the stationary position;

2) the q^2 dependence was checked for **q** lying in the interface plane;

3) the measured linewidth was about 3.5 times smaller than that measured by Bilgram's group for crystals growing along the c axis, indicating that whatever is the nature of the scatterers their lifetime is longer at the a face of the crystal than at the c

face.

B. Salol Crystal-Melt Interface Experiment

Experiment performed by U.Durig and J.H.Bilgram[8,9]

The first results on light scattering at the crystal-melt interface of the organic crystal Salol was reported by U.Durig and J.H.Bilgram[8] in 1982. They observed two different dynamical processes; one manifests itself by an oscillatory intensity autocorrelation function and the other by an exponentially decaying one, similar to the ice-water case. The main results from that experiment were :

1) there was a critical growth velocity for the onset of the scattering which was about 0.2 $\mu m\ s^{-1}$;

2) for $0.2<v_G<0.4\ \mu m\ s^{-1}$ the scattered intensity was highly anisotropic in space and its autocorrelation function was sinusoidal and undamped;

3) if v_G was increased above 0.4 $\mu m\ s^{-1}$, the oscillatory correlation function became damped and after about 2 hours it disappeared while an exponentially decaying one emerged. The scattered intensity was then isotropic in space and very similar to the one found in the ice-water experiment.

They interpreted the oscillatory correlation function as the result of beating between elastic scattering and light scattered from the interface with a Doppler shift $\Delta\omega = \mathbf{v}_L.\mathbf{q}$. The linear dependence on $\mathbf{q}$ was verified and the velocity v_L shown to be about

60 μm s^{-1}, which was 150 times larger than the growth velocity v_G.

Recently Durig[9] interpreted these results as being caused by the motion of the ledges of screw dislocations in agreement with our earlier[11] interpretation, which will be discussed in the next sections of this thesis. By using the evanescent wave as a probe for the scattering in the boundary layer and from the analysis of the scattered intensity, Durig concluded that the width of the boundary layer was of the order of 1 μm.

IV. SALOL

A. Crystal structure

The crystal structure of Salol (benzoic acid 2-hydroxy phenylester or phenyl salicylate, $C_{13}H_{10}O_3$) has been determined by Flachsbart[50] and refined by Bilgram et al.[51]. Salol is a very anisotropic crystal with an orthorombic unit cell. A typical Salol crystal grown from solution is shown in Figure 4.1 . The cell dimensions recorded at -80°C are[51],

$a = 11.258$ Å , $b = 23.402$ Å and $c = 7.961$ Å .

At room temperature the values are[50],

$a = 11.25$ Å , $b = 25.50$ Å and $c = 8.10$ Å

The convention of axes chosen by us is different than that of Bilgram et al. The distances as well as the angles between the atoms are described in Bilgram's work[51].

B. Refractive indices

1) melt

The refractive index of the Salol melt was measured using the minimum deviation technique. The melt at about 45°C was poured into a prismatic cuvette. The temperature was not controlled during the experiment, therefore the value obtained for the refractive index was an average over a range of temperatures. The prismatic cuvette was mounted on a goniometer and the laser beam at $\lambda = 488$ nm was refracted through the prism. With the goniometer we could measure the angles of the prism as well as the angle of

incidence for the condition of minimum deviation of the refracted beam. By using the well known formula from the optics of the prism,

$$n = \frac{\sin\delta}{\sin(\frac{A}{2})}$$

where n is the index of refraction of the prism, A is the apex angle of the prism and δ is the angle of incidence for the condition of minimum deviation, the resulting index of refraction for the melt was

$$n_m = 1.598 \pm 0.008$$

(2) crystal

The method used to measure the indices of refraction of the crystal was the prism method. Oriented Salol crystals were cut in prisms with one of the faces normal to one of the crystallographic axes. By using the incident beam with λ = 488 nm normal to this face, so that the propagation direction is along one of the axes of the crystal, there are two solutions to the Maxwell's equations for propagation inside of the crystal, producing two beams refracted out of the prism. Since Salol has an orthorombic unit cell the principal optical axes are orthogonal to each other. Therefore the two beams refracted out of the prism have mutually orthogonal polarizations. With Snell's law we can obtain the desired indices of refraction. With this procedure we need two different prisms oriented in different ways to obtain the three indices of refrac-

tion. These measurements were performed by M. Awal and are described in his Ph.D. thesis[52]. The results were:

$n_a = 1.66 \pm 0.02$ $n_b = 1.83 \pm 0.03$ $n_c = 1.55 \pm 0.02$

C. Sample preparation

The sample preparation followed essentially the procedure of Bilgram et al.[51]. The procedure can be described in the following steps :

(1) Starting seeds

The Salol used in the experiment was stock material purchased from Eastman Kodak in powder form. In a small jar imersed in a thermostated water bath at 40°C we dissolved 25 grams of Salol in 100 ml of pure ethanol. The supersaturated solution was then poured into a glass dish. The dish was kept in a quiet environment with a loose cover, for about 2 days. The natural decrease of the temperature of the solution and the evaporation of part of the ethanol are sufficient to let small Salol seeds grow on the bottom of the dish. These are good starting seeds.

(2) Bridgman growth technique

We chose a good starting seed and polished it to have a cylindrical shape with the face of interest at the ends of the cylinder. This cylindrical seed fit in a pyrex growth tube whose bottom diameter is about 5 mm; the main part of the tube had a diameter of about 18 mm. After setting the seed in place the tube was filled with Salol powder and was mounted in the apparatus shown in Figure 4.2 . The Salol powder was melted back to the top of the seed. Since the seed was very small this step must be done

very carefully to avoid melting the seed. The motor was then turned on allowing the growth tube to move downward through the temperature gradient and the crystal growth to proceed. We typically used a growth velocity of 0.08 μm/s. When the length of the crystal was about 10 cm we stopped the growth.

(3) Preparing the starting crystals

In the apparatus shown in Figure 4.3 a), the growth tube can be placed in an upside-down position. (The figure illustrates another use of the same apparatus to be discussed below). When water at 42°C was circulated through the apparatus the crystal became loose and slid down out of the growth tube. After this step we had a single crystal of 10 cm length, with the facet of interest roughly normal to the axis of the cylindrical crystal. Subsequently, this crystal was cut in pieces of 2 cm height. Because the next step in sample preparation (orienting the starting crystal) required that these 2cm high cylindrical crystals have well developed facets, we had to reinsert them in another Salol-ethanol solution for the facets to grow. This supersaturated salol-ethanol solution (50 gr Salol/ 100 ml ethanol) was prepared at 40°C. At this concentration and at a temperature of about 27°C, Salol crystals will grow. Before inserting the starting crystal in the solution, we checked the conditions of growth using a test seed. Temperature adjustments were then made to obtain the most convenient growth conditions. We chose one of the 2 cm cylindrical pieces and immersed it in the solution. The cylindrical crystal began to develop facets and to grow. By decreasing the bath temperature by 0.2°C/day, after 3 or 4 days the cylindrical crystal developed good

facets. It was removed from the solution and imediatly, with a lens paper, the remaining solution was removed from the facet of interest.

(4) The main growth tube

The main growth tube, i.e., the tube which was actually used for the light scattering experiment, was made of pyrex. The length is about 35 cm, the internal diameter 16 mm and the external diameter 18 mm. There is a built-in stopcock to allowing the sample to be kept under vacuum. It is with this type of tube that we have obtained most of our results. Recently we have changed to heavy wall tubes, but with the same internal diameter, because we had problems due to cracking of the tube inside of the thermostat. With the use of heavy wall tubes we had to increase the diameter of the bore of our thermostat. This has caused a worsening in the fit of the measured temperature profiles.

(5) Orienting the starting crystal

Using undercooled Salol at room temperature, we "glued" the starting crystal to the top of a small goniometer which can be mounted in a lathe. With the help of a small He-Ne laser aligned along the axis of the lathe, we adjusted the setscrews of the goniometer, such that the laser light was reflected back from the facet on the end of the cylindrical starting crystal which oriented this facet normal to the axis of the lathe. After that we machined the starting crystal down. The machining was done very slowly in very small steps to avoid cracking the crystal. When the crystal fit snugly in the main pyrex growth tube whose internal diameter is about 16 mm, we stopped the machining. With this pro-

cedure the facet of interest was normal to the axis of the growth tube within ±1°. The starting crystal was then inserted in the main growth tube where it became the new seed for melt-growth, and the bottom of the tube was blown closed.

(6) Vacuum distillation

In our vacuum distillation apparatus the "raw" Salol was double distilled at a temperature of 115°C. The main growth tube was then mounted in the distillation apparatus and Salol was distilled into the tube (3rd. distillation). When enough Salol has been distilled into the tube, the sample was sealed under vacuum by closing the built-in stopcock.

(7) Growing the crystal in the main apparatus

In the main apparatus we again used the Bridgman technique to grow the crystal. The growth tube was mounted in the main crystal growth apparatus where the light scattering experiment was performed. This apparatus will be decribed later. After mounting the growth tube in the main apparatus the distilled Salol was melted by slowly raising the tube until the top of the growth seed was reached. Initially a slow growth velocity was set (typically 0.0423 μm/s) until a clean flat interface formed. After that, a desired growth velocity could be set. Since this was the first pass of the crystal in the apparatus, we kept a constant growth velocity of 0.08 μm/s until the end of this pass.

(8) Zone refining the seed and the crystal

After the first pass we had a solid single crystal inside of the growth tube. To perform zone refining we had to melt a zone close to the seed. An empty space between the seed and the bottom

of the tube was necessary to avoid cracking of the tube due to the expansion of the Salol during melting. This space was provided by shifting the whole crystal using the apparatus used in step (3) and shown in Figure 4.3 a). Our procedure of melting a zone was different than that used by Bilgram et al.[51]. In the apparatus shown in Figure 4.3 b), we mounted the growth tube in an upside-down position, such that the whole seed was about 1 cm above the aluminum heating plate. With water circulating at 42°C in the glass jacket, the parts of the crystal in contact with the walls melted slightly. After that we set the temperature of the thermostated aluminum plate to 48°C and a zone started to melt without building up pressure in the tube, since the melt could flow up to the empty space above the seed. Before the zone had been melted completly, to prevent having the seed fall down, we decreased the temperature of the circulating water to 38°C. By doing so the seed became attached to the growth tube again. Subsequently the temperature of the heating aluminum plate was decreased to 45°C and we waited until the zone had been completly melted. We set the growth tube to move downward, and the melted zone advanced through the seed, zone refining the seed. This procedure improves the quality of the seed. If the tube was set to move upward, the crystal would be zone refined. By removing the last 2 cm of the crystal, which contains most of the impurities and replacing it by freshly distilled Salol, the purity of the crystal is improved.

We did not perform the zone refining of the seed after every pass. But after every pass in the main apparatus we removed the last 2 cm of the crystal and we replaced it by freshly distilled

Salol. So the purity of the crystal was continuously improved as the experiment progressed. We have found that after 4 passes the quality of the crystal-melt interface was satisfactory for light scattering experiments. Our main set of data was obtained between the fifth and tenth passes of one of our crystals.

V. APPARATUS

A. General Description

We have constructed a light scattering spectrometer for investigating the crystal-melt interface based on the apparatus of Bilgram's group, but incorporating several important modifications.

The overall layout is shown schematically in Fig. 5.1 and the thermostat is shown in Fig. 5.2 .

1) Laser:

The laser used was a Spectra Physics 165 Argon Ion Laser operating in single mode at λ = 488 nm. The laser power incident on the sample throughout the experiment was always less than 50 mW.

2) Optical Table:

The whole apparatus was mounted on a Modern Optics Vibration Isolation Table Model ST-40E/S-4.

3) Optics:

The laser is focused by a 40 cm. focal length lens (L1) into the growth tube containing the sample. Variable attenuation is provided by the rotatable half wave plate (λ/2), and linear polarizer (P1).

Light scattered through an angle θ relative to the reflected beam (measured in the horizontal plane) passes through a 1 mm. diameter pinhole (A1) and the scattering volume is imaged by an 18 cm. focal length lens (L2) on the 100 μm diameter pinhole (A2). The size of the pinholes are determined in such a way as to collect as much scattered light as possible within a single coherence area.

For the maximum signal-to-noise ratio, only one coherence area must illuminate the photomultiplier tube (PMT).

4) Photomultiplier and Amplifiers:

The photomultiplier (PMT) used was an ITT FW130. The output of the PMT was amplified by a factor of 10 by a LeCroy preamplifier model A1007, which was located inside the housing of the PMT. The preamplifier output signal passes through a shielded 50Ω coaxial cable to a LeCroy 2-stage fast linear amplifier model 133B, followed by an EG&G discriminator model T105/N. The gain setting of the amplifier together with the discriminator threshold was adjusted to have as much signal as possible without a great amount of noise. The gain was set to 24 and the discriminator threshold to 40 mV. The discriminator output consists of standardized 1.2V negative pulses of 12 nanoseconds width for each input pulse above the threshold voltage. The output of the discriminator is then fed into the autocorrelator.

5) Autocorrelator:

The autocorrelator used is a 60-channel digital instrument designed by A. Frazer and built by the Applied Physics Laboratory at Johns Hopkins University. It has single clipping, double clipping, prescaling and multiscaling capabilities. It also provides the option of having the last 16 channels delayed in time for more accurate determination of baselines. The clipping mode should only be used for signals whose electric field amplitude distribution follows Gaussian statistics. That is in general the case of scattering of light by fluctuations in the dielectric constant caused by diffusive dynamics. In the case of Doppler-velocimetry

measurements, where a strong local oscillator is present, the statistics are no longer Gaussian and the prescaling mode must be used in place of the clipping mode. The available clipping levels are 0, 1, 3, 7, 31, 127, 511 and 2047. The available prescaling levels are 2, 4, 8, 16, 64, 256, 1024 and 4096. The autocorrelation sampling time can be varied from 50 nanoseconds to 2 seconds. The duration time of a run can be selected from 5×10^{-7} to 2×10^{5} seconds. The autocorrelator is interfaced to a PDP8E minicomputer which will be described later.

6) Rotary Stage System:

The pyrex growth tube can be rotated about its axis by a Rotary Stage (Daedal Inc. Model 20000) driven by a Superior Electric SLO-SYN synchronous/stepping motor type M062-FD03 and a Superior Electric SLO-SYN Translator Model ST 101. The Translator is interfaced to the PDP8E minicomputer such that the rotation of the growth tube can be computer controlled.

7) Computers:

The PDP8E minicomputer is interfaced to both the autocorrelator and the rotary stage system. The PDP8E sends a start pulse to the autocorrelator to initiate a run. After each run the data is transferred to the PDP8E and stored in its memory. The number of runs can be programmed, so a continuous stream of data can be accumulated. The data can subsequently be transferred to the Science Division's main frame PDP10 computer for storage and analysis. We can also program the PDP8E computer to rotate the growth tube between the runs which proved to be useful in the experiment. The software for all these capabilities was developed

here in the Physics Department, and all the versions currently in use in different laboratories belong to the same family of ZAP Programs.

8) Vertical Motion Drive System:

In the Bridgman technique of crystal growth the growth tube must be lowered in a temperature gradient for the crystal to grow. This motion must be as uniform and smooth as possible to obtain crystals of good quality, and accurate enough to allow quantitative studies of the growth velocity of the crystal. In our apparatus, which was designed and constructed by Mr. R. Quinlan, vertical motion is provided by a precision stainless steel drive screw purchased from Winfred M. Berg Inc. driven by a synchronous motor (Insco Co. Model 06700-4S). This model includes a gear box such that the motor and the gear box are parts of the same unit. Through a second gear box (Insco Co. Model 00143) with selectable gear ratios the drive train provides 28 different growth speeds ranging from 0.00423 μm/s to 8.467 μm/s.

B. Thermostat, Temperature Controllers and Temperature Monitoring System

The thermostat is shown in Fig. 5.2 . It is constructed from two cylindrical aluminum blocks whose heights are 4.5 cm and external diameters 10.2 cm, separated by a plexiglas cylinder whose height is 5.7 cm and external diameter 5.1 cm. The diameter of the bore of the aluminum and plexiglas cylinders is 1.9 cm which is large enough for the growth tube to slide freely. The bore was filled with paraffin oil for thermal contact and for ref-

ractive index matching.

In the upper aluminum block, which is kept above the melting temperature of Salol, we inserted two heaters purchased from Hotwatt Inc. In the lower aluminum block, which is kept below the melting temperature of the Salol, a canal was drilled to allow water to be circulated for temperature controlling purpose. The upper aluminum block temperature TU is controlled by a YSI Proportional Temperature Controller Model 72. The lower aluminum block temperature TL is controlled by water from a Lauda Refrigerated Circulator Model K-2/R.

Since the thermal conductivity of the plexiglas is low, the radial heat flow caused by convective heat transfer to the room at temperature TA was comparable to the vertical heat conduction through the plexiglas cylinder. At our operating temperatures, the room temperature was always smaller than TL, causing a hook shape vertical temperature profile, unacceptable in our experiment. To avoid this situation, it is necessary to have TA always larger than TL which was achieved by blowing filtered temperature-controlled hot air inside of the thermostat. To keep the azimuthal symmetry the blown air should be uniformly distributed around the plexiglas cylinder. This was accomplished with the use of a teflon ring with evenly-spaced small holes surrounding the plexiglas cylinder. To keep the air moving past the plexiglas as well as to provide an escape for the blown air, a glass sleeve was mounted around the plexiglas with a free space of about 1 mm from the lower block. The temperature of the blown air was controlled by a Cole-Parmer Versa-Therm Proportional Temperature Controller Model 2156.

The temperature profile was measured by a set of ten calibrated thermistors (Omega Model 44018), which were embbeded in the plexiglas cylinder spaced 0.5 cm from each other and located at 1.27 cm from the axis of the cylinder. Their resistances were sequentially scanned by an Omega Automatic Signal Scanner Model DataPlex-10, and the conversion from resistance to temperature readings was made by a calibrated Omega Digital Temperature Indicator Trendicator Model 410A-THC, which also provides a continuous output signal for the Strip Chart Recorder (Honeywell Model Electronik 193).

VI. EXPERIMENTAL PROCEDURE

A. General Procedure

In the thermostat of Fig. 5.2 , the bore of the plexiglas and aluminum cylinders is filled with paraffin oil which maintains thermal contact to the growth tube and also provides optical index matching.

The temperatures of the upper and lower aluminum cylinders as well as the temperature of the circulating air, TU, TL and TA respectively, are chosen to minimize the radial heat flow at the interface and at the same time to have the interface at steady state approximately at the middle of the thermostat. The radial heat flow at the interface will be zero if the temperature of the interface T_i is equal TA. The interface will be at the middle of the thermostat if T_i = (TU+TL)/2. Thus we try to work as close as possible to the condition

$$T_i = TA = (TU+TL)/2$$

Typical values for these temperatures are TU = 43.5°C, TA = 39.5°C and TL = 35.5°C. The thermistor readings are continuously monitored by the strip chart recorder.

After mounting the growth tube in the apparatus, it is initially driven upward until the crystal melts back to the top of the surface of the growth seed. The growth velocity v_G is then set at a low value (typically 0.0423 μm/s) and the tube is driven downward until a clean flat crystal-melt interface forms. The growth velocity v_G is then set to the desired value for the experiment. After one day, steady-state is reached and the interface then remains stationary in the laboratory frame. The position of

the interface with respect to the thermistors is measured within ± 0.1 mm by a traveling microscope. The growth velocity v_G is equal (and opposite) to the downward tube velocity. However, during the day there is a small drift in the room temperature which causes a small drift in the temperature of the thermostat. The interface starts moving in relation to the laboratory frame, seeking a new steady-state position. By recording the position of the interface every half-hour, the velocity of the interface in relation to the laboratory frame can be calculated. With the help of the expression,

$$\Delta v = v_G - v_T$$

where Δv is the velocity of the interface in relation to the laboratory frame, v_G is again the growth velocity of the crystal and v_T is the downward tube velocity, we can obtain the correct v_G.

The power of the laser beam used throughout the experiment was always smaller than 50 mW. In order to precisely locate the position of the a axis of the crystal for growth parallel to the b axis, the beam is focused onto the interface from slightly below the horizontal, near grazing incidence, with horizontal polarization. The refractive indices of Salol are $n_a = 1.66$, $n_b = 1.83$, $n_c = 1.55$ and $n_m = 1.60$. As the sample tube is rotated about its axis, the horizontal polarized beam is transmitted through the interface into the melt when the a axis is in or near the plane of incidence. The angle of rotation of the tube about its axis at which the beam crosses the interface at maximum angle above the horizontal precisely locates the orientation of the a axis of the crystal.

Both homodyne and heterodyne detection configurations were used. The homodyne configuration is the one shown in Fig. 5.1 . For the heterodyne configuration a beam spliter is used before lens L1 to provide an external local oscillator. The intensity of the external local oscillator is adjusted by adding neutral density filters. A second beam spliter is used before pinhole A1 in such a way that the external local oscillator and the scattered light are combined to pass through the collection optics and beat at the photomultiplier tube.

Depending on the scattering geometry, two different dynamical processes can be observed: one manifests itself by a oscillatory intensity autocorrelation function (from now on referred to as oscillatory scattering) and the other manifests itself by a relaxational intensity autocorrelation function (from now on referred to as relaxational scattering). These two dynamical processes coexist and can be studied separately. The scattering geometries are shown in Fig. 6.1 .

B. Geometry to observe oscillatory scattering

The vertically polarized incident beam is focused onto the interface from slightly below the horizontal. Since n_b is considerably larger than n_m, the beam is always totally internally reflected at the interface for our working incidence angles. The scattered light is also collected from below the horizontal, so that the optical path is completely within the crystal. The growth tube must be rotate about its axis until scattered intensity is observed. The intensity autocorrelation function is oscillatory and

undamped as shown in Fig. 6.2 . This scattering is extremely anisotropic; in a given run it is only observed when the scattering wave vector **q** is oriented in a particular direction β relative to the a axis of the crystal to within ± 2° . However, on successive runs β is often different. Most frequently β is approximately 54° or 35° corresponding to crystallographic directions <101> or <201>. This scattering only appears when the growth velocity is increased to at least 0.1 μm/s, but persists when v_G is subsequently decreased to the lowest accessible values. Both homodyne and heterodyne detection configurations were used to study this scattering. The data was obtained for crystals growing along the b direction. For crystals growing along the a direction the presence of large lateral facets usually made observations impossible. In addition, since n_a is not much larger than n_m, the evanescent waves have a considerable penetration depth at our working angles. The evanescent waves therefore acted as a probe for the scattering occurring in the layer between the crystal and the melt, which will be discussed next, superimposing the oscillatory and relaxational scatterings.

C. Geometries to observe relaxational scattering

If we use the geometry described in B but change the polarization of the incident beam to horizontal, as the growth tube is rotated about its axis the beam can go from a situation of total internal reflection to a situation of partial transmission at the interface. The change from total internal reflection to partial transmission as a function of polarization and crystal rotation provides the key to identifying the origin of the different types

of scattering that we observe.

When the beam is transmitted through the interface, very strong isotropic scattering is observed. The intensity autocorrelation function is relaxational as can be seen in Fig. 6.3 . The same type of scattering is observed if the incident beam, with any polarization, is focused onto the interface from above the horizontal and the scattered light is also collected from above the horizontal, such that the optical path is completely within the liquid. Therefore, this scattering could be associated with some process in the bulk melt. However, it is only observed if the beam actually touches the interface, indicating that there is a thin boundary layer between the crystal surface and the bulk melt with completely different properties than those of the bulk melt. Therefore our results confirm Bilgram and Boni's conclusions about the existence of a boundary layer[7].

Although weak at low growth velocities, this scattering was observed for growth velocities as small as 0.04 μm/s. The scattered intensity increases with velocity. Data was collected and stored for both crystals growing along the a and b directions using both homodyne and heterodyne detection configurations.

D. Relaxational scattering when the crystal is melting

If instead of moving the sample tube downward we set it to move upward, the crystal will start to melt. As in the growing case, a steady-state situation of melting can be achieved. The interface, however, is not flat, but follows an isotherm of the thermostat. Nevertheless light scattering could be performed with

the beam incident from the liquid side just touching the highest point of the rounded interface. We again observed a relaxational intensity autocorrelation function with the same characteristics as those observed when the crystal was growing. The only noticeable difference compared to the growing case is the higher melting velocity for the onset of the scattering, which we have found to be about 0.5 μm/s. This scattering was observed for crystals melting along both the a and b directions.

E. The two dynamical processes

From the above observations we concluded that two different dynamical processes are occurring simultaneously at the crystal-melt interface of Salol and that they can be studied separately. The oscillatory scattering reveals a dynamical process occurring at the crystal surface whereas the relaxational scattering reveals a dynamical process occurring in a thin boundary layer between the crystal surface and the bulk melt. By choosing the appropriate geometry, each of these dynamical processes can be studied independently.

VII. Results

A. Crystal surface dynamics

In Figure 6.2 the experimental data is represented by the circles. The solid line is a computer fit to

$$C(\tau) = B + A \cos(\omega\tau)\, e^{-\Gamma\tau}$$

The expression for the Doppler shift of the light for velocities small compared to the velocity of light is given by,

$$\omega = \mathbf{v}_L \cdot \mathbf{q} \; . \qquad 7.1$$

If we assume that there are growth steps moving laterally across the surface of the crystal with velocity v_L parallel to the projection of $\mathbf{q}$ on the interface, expression 7.1 can be written as,

$$f = (2\, v_L \frac{n}{\lambda_0}) \cos\psi \sin(\frac{\theta}{2}) \qquad 7.2$$

where we have used $f = \omega/2\pi$, λ_0 is the laser wavelength, n is the index of refraction of the crystal, ψ is the angle between the incident laser and the interface, and again θ is the scattering angle. The plot of frequency f vs. $\sin(\theta/2)$ for fixed ψ is shown in Figure 7.1 . The circles are the experimental data and the straight

line is the Doppler shift prediction of Eq.7.2 . We thus interpret the data, following Durig and Bilgram[8], as indicating motion with velocity v_L in the plane of the interface which Doppler shifts the scattered light. Beating of this light with elastic scattered light (probably stray light from the crystal interface) at the phototube produces the oscillating correlation function. The absence of damping ($\Gamma \sim 0$) indicates that v_L is very well defined. To assure that the beating was with elastic scattered light, we used an external local oscillator in a standard heterodyne configuration. No change in frequency of the oscillation was observed. Analysis of the data yields values of v_L as a function of v_G and the undercooling ΔT.

B. Boundary Layer Dynamics

The exponentially decaying intensity autocorrelation function of the scattered light from the boundary layer was fit to a superposition of exponentials by a computer fitting program which performs a cumulant analysis of the data. From the fitting we conclude that the relaxational intensity autocorrelation function is a single exponential to within experimental error, since the polydispersity index μ_1/μ_2^2 was usually less than 10%. In Figure 6.3 the data (circles) are a fit to

$$C(\tau) = B + A\, e^{-2\Gamma\tau}$$

The decay constant Γ is proportional to q^2 ($\Gamma = Dq^2$) where D plays

the role of a "diffusion constant", for **q** lying nearly in the interface plane. We did not check the q^2 dependence for **q** normal to the interface. This relaxational scattering was observed in crystals growing along both the b and a axes and was also observed when the crystal was melting along either direction. We did not find any clear correlation between the decay constant and the other parameters of the experiment. We summarize our results in the table below showing the values of the "diffusion constant" D in cm^2s^{-1} for melting and growth along different axes of the crystal.

	growth	melting
a-axis	$0.6\times10^{-10} < D < 1\times10^{-10}$	$0.8\times10^{-10} < D < 1\times10^{-10}$
b-axis	$1\times10^{-10} < D < 1\times10^{-9}$	$1\times10^{-10} < D < 3\times10^{-10}$

The data for crystals growing along the b axis corresponds to measurements on five different samples whereas the other sets of data correspond to measurements on one sample oriented along the b axis and another one oriented along the a axis.

As mentioned previously, the main difference between the scattering when the crystal is growing and the scattering when the crystal is melting is that in the former the critical velocity for the onset of the scattering is about 0.04 $\mu m\ s^{-1}$ whereas in the latter this critical velocity is about 0.5 $\mu m\ s^{-1}$.

In an attempt to improve the quality of the data we used a heterodyne configuration, which was described previously. No measurable improvement was obtained.

C. Measuring the undercooling ΔT

The parameter ΔT is the difference between the melting temperature and the actual temperature of the interface. It is very difficult to obtain the temperature of the interface, since the crystal liberates latent heat during the solidification process. We cannot insert a probe inside the crystal close to the interface, because it would disturb the growth process. To minimize the latent heat problem, capillary tubes are usually chosen for experiments in crystal growth. We cannot adopt this solution in light scattering experiments. In the case of larger tubes one can try a theoretical treatment of the heat transfer in the growth tube and infer the temperature of the interface from the external temperature readings. This is the approach we used. The temperature readings of ten thermistors embedded in the plexiglas cylinder were fit to a theoretical expression which takes into account the heat transferred to the ambient air by convection and also takes into account the latent heat liberated at the interface of the crystal. We used a Non-Linear Least Square Fitting computer subroutine to fit the data. A typical temperature profile measured by the thermistors (circles) and the theoretical fit (continuous line) is shown in Figure 7.2 . Details of the calculation are given in Appendix A.

VIII. Interpretation

A. Crystal Surface Dynamics

Salol is a crystal with Jackson α-factor ~ 5. A lateral growth mechanism rather than a continuous one is to be expected[13]. The oscillatory correlation function we observed suports this idea, since the Doppler shift of the light is caused by steps moving across the interface with velocity v_L. Therefore the crystal is growing either by nucleation or by a screw dislocation mechanism.

1) Kinetics of the growth

Recalling from chapter II the kinetic equations for these two mechanisms, we have:

$$v_G = \mu_2 \exp(-\frac{K}{\Delta T}) \qquad 2.2$$

$$v_G = \mu_3 (\Delta T)^2 \qquad 2.3$$

Since the step edge is "rough" for all temperatures, for small ΔT a linear kinetic equation holds for the lateral growth[15]:

$$v_L = \mu_L \Delta T \qquad 8.1$$

Combining equations 2.2 and 8.1, we obtain for nucleated layer growth,

$$v_L = \frac{K\mu_L}{\ln(\frac{\mu_2}{v_G})} \qquad 8.2$$

Combining equations 2.3 and 8.1, we obtain for screw dislocation growth,

$$v_L = \mu_L(\frac{v_G}{\mu_3})^{0.5} \qquad 8.3$$

In attempting to fit our experimental data to equations 2.2, 2.3, and 8.1, 8.2 and 8.3, the temperature dependence of the viscosity was first divided out to isolate kinematic effects on the crystal surface[33]. The velocities were corrected by using the following expression:

$$v_c = v \frac{\eta(Ti)}{\eta(41.21^{\circ}C)}$$

where v_c is the corrected velocity, v can be either v_L or v_G, and η is the viscosity of the Salol melt. The viscosity data used was obtained by O. Jantsch[53]. In the temperature range of interest, the viscosity data of Jantsch as a function of temperature was fit to the following polynomial:

$$\eta(T) = 0.755 - 3.42\times10^{-2}T + 5.85\times10^{-4}T^2 - 3.53\times10^{-6}T^3$$

with η in poise and T in $^{\circ}C$. This corresponds to a correction of

about 8% for the highest velocity. Fits of v_G vs. ΔT were not able to distinguish between nucleation and screw dislocation mechanisms (eqs. 2.2 and 2.3) due, in part, to the uncertainties in ΔT. Fits of v_L vs. v_G following equations 8.2 and 8.3, gave better agreement for the screw dislocation mechanism than for surface nucleation as shown in Figure 8.1. Also, a fit to $v_L = C(v_G)^n$ gave,

$$v_L = (62\pm2)v_G^{(0.50\pm0.02)} \ \mu m \ s^{-1}$$

with n = 0.50, the value predicted by equation 8.3. The data and computer fit of v_L vs. ΔT using equation 8.1 is shown in Figure 8.2. From this fit the lateral kinetic coefficient and the melting temperature were:

$$\mu_L = 22\pm1 \ \mu m \ s^{-1}K^{-1} \text{ and } T_m = 41.21\pm0.07 \ ^{\circ}C.$$

Values for the normal kinetic coefficient μ_3 were obtained from either equation 2.3 or from equations 8.1 and 8.3. The results were $\mu_3 = 0.129$ and $0.124 \ \mu m \ s^{-1}K^{-2}$, repectively, showing the self-consistency of the proposed interpretation. These values for μ_3 are in qualitative agreement with the value obtained by Ie and Strickland-Constable[35] for growth along the b axis of salol. They found for free-growing Salol $\mu_3 \sim 0.1 \ \mu m \ s^{-1}K^{-2}$. They did not take into account the latent heat generated at the interface in their measurements of the undercooling.

2) Morphology of the Spiral

Screw dislocations produce spirals which spread across the crystal surface. The spirals can be either round or polygonized, depending on the crystal structure and driving force[27]. Very anisotropic crystals with high Jackson α-factor tend to exhibit highly polygonized faceted growth spirals, consistent with the observed highly anisotropic light scattering. Geometrically, the relation

$$\frac{v_L}{v_G} = \frac{w}{h} \qquad 8.4$$

should hold, where w is the horizontal distance between the arms of the spiral and h is the height of the steps. Typically, w/h ~ 10^2 - 10^3 for solution growth, ~ 10^3 - 10^4 for vapor growth[27]. From our measured values of v_L and v_G, w/h ~ 600 for the smallest v_G and ~ 100 for the largest v_G. The magnitude of the Burgers' vector of the dislocation is given by the height of the step divided by the lattice constant. Therefore if h is one lattice constant, the magnitude of the Burgers' vector of the dislocation is one. Dislocations with large Burgers' vectors are generally energetically unstable and decay into multiple smaller dislocations[27]. Assuming that in our case h corresponds to one lattice constant h = 25.5$\mathring{A}$, at maximum undercooling (ΔT ~ 2 K), w ~2500$\mathring{A}$ which comes close to satysfying the Bragg condition for diffraction. We observed large changes in the intensity of scattering from the crystal surface which can be understood in terms of nearly constructive interference in scattering from successive steps. Optically the steps ori-

ginating at the screw dislocations act as a moving line diffraction grating. Durig[9] studied the Bragg peaks produced by this structure and was able to obtain the distance w between the steps of the screw dislocations. Therefore in his experiment he had the parameters v_G, v_L and w. By applying the relation 8.4 he obtained an average step height of 2.5±0.8 lattice constants. If we use his result at our maximum undercooling, our w would be of the order of 6000Å .

Theoretically, the step width w is related to the radius r* of a critical nucleus for two-dimensional nucleation by,

$$w = sr^* \tag{8.5}$$

where s = 5.4 for polygonized monomolecular spirals and s = 19 for round monomolecular spirals[27], monomolecular spirals meaning spirals with step height one Burgers' vector.

$$r^* = \frac{\sigma V_m}{\Delta S \Delta T} \tag{8.6}$$

where σ is the step free energy, V_m is the molar volume, ΔS is the molar entropy of melting, and ΔT is again the undercooling. If we substitute 8.6 and 8.5 in 8.4 we obtain

$$\frac{v_G}{v_L} = \frac{h \Delta S \Delta T}{s \sigma V_m} \tag{8.7}$$

Since we did not find a value for σ of Salol in the literature, we estimated its value by using Turnbull's formula[54] for organic materials:

$$\frac{\sigma V_m}{d} \sim \frac{T_m \Delta s}{3} \qquad 8.8$$

where d is the molecular dimension along of the direction considered. Substituting 8.8 in 8.7 and using the result for Salol along the b direction h = 3d, we obtain the expression,

$$\frac{v_G}{v_L} \sim 9 \frac{\Delta T}{s T_m} \qquad 8.9$$

From the fit of v_G/v_L vs. Ti using equation 8.9, we obtained

$$\frac{v_G}{v_L} = (5.8 \pm 0.3) 10^{-3} (41.22 \pm 0.01 - Ti)$$

From this result we can calculate the value of s. The value obtained was,

$$s \sim 5$$

which is very close to the value for polygonized spiral. (If we use the value h=2.5 lattice constants reported by Durig we obtain the value s ~ 12.) Equation 8.5 with s=5.4 or s=19 is valid for monomolecular single spirals and in our calculations of s the value for

σ was estimated from Turnbull's relation. Nevertheless the estimated values for s are in reasonable agreement with the theory. From the strong anisotropy of the scattered light and from the estimated values for s, we thus conclude that the observed translational dynamics on the crystal surface result from crystal growth mediated by highly polygonized screw dislocations with prominent <101> or <201> facets.

One possible cause for the large scatter in the data of v_L versus v_G is the fact that the concentration of screw dislocations is a parameter which we cannot control in the experiment. As discussed in Chapter II, in real crystal growth there are a great number of screw dislocations interacting with each other in the surface of the crystal. These interactions change the distance between the arms of the spiral. The value s=5.4 for the ideal case of a single polygonized spiral changes if more screw dislocations are present. In general, as the number of screw dislocations increases the value of s decreases. Therefore the kinetic coefficient μ_3 may vary from one experimental run to another in an uncontrollable way, giving rise to the spread in the data of v_L versus v_G. The relationship between v_L and ΔT should not be affected by the change in concentration of screw dislocations. However, as pointed out previously, ΔT is not easy to determine from the temperature readings, and the resulting values are subject to large uncertainties.

B. Boundary Layer Dynamics

The following properties of the relaxational scattering have now been established:

(a) It occurs when the crystal is either melting or growing.

(b) The critical velocities for the onset of the scattering are about 0.5 μm/s when the crystal is melting and 0.04 μm/s when the crystal is growing.

(c) It originates in the fluid boundary layer and coexists with translational dynamics on the crystal surface.

(d) It is much stronger than scattering from the bulk fluid.

(e) The correlation function, to within experimental error, is described by single exponential relaxation.

(f) The relaxation rate $\Gamma = Dq^2$.

(g) D is independent of the growth rate.

To explain these observations, several mechanisms can be considered:

(1) The corrugated surface model originally proposed by the ETH group, is ruled out by (c) and (f), despite the remarkable agreement with the Gibbs-Thomson equation.[4,5]

(2) Formation of clusters of precrystalline material near the interface would explain all the data. However, the observed values of D imply clusters of more than 3000Å radius, and (e) implies little or no variation in cluster size, both of which seem highly improbable.

(3) Small-scale turbulence within the boundary layer. The intensity autocorrelation function of the light scattered by particles suspended in a turbulent fluid was calculated by Di Porto et al.[55]. The decaying intensity correlation function is q^2 dependent but the

temporal dependence can be linear or quadratic for two limiting cases. For $t << t^*$, where t^* is the time for which the Lagrangian correlation function of velocities of the turbulent flow is practically zero, the temporal dependence is quadratic and so the intensity autocorrelation function of the scattered light is a Gaussian function of time. In the other limit $t >> t^*$, the intensity autocorrelation function of the scattered light is exponential in time. Crosignani et al. (in Ref. 43) have pointed out that $t^* >> (q^2\langle v^2\rangle)^{-0.5}$ in practical cases. $(q^2\langle v^2\rangle)^{-0.5}$ is of the order of the decay time of the intensity autocorrelation function, where $\langle v^2\rangle$ is the mean square value of the velocity of the turbulent flow along **q**. Therefore in practical situations $t\tau\ (q^2\langle v^2\rangle)^{-0.5} << t^*$, and hence the intensity autocorrelation function of the scattered light is Gaussian in time. Another difficulty with the small-turbulence model is that it cannot explain the enhancement of the intensity of the scattered light from the boundary layer compared to that of the bulk melt. Therefore this model is weakened by (e) and probably ruled out by (d).

(4) Structure within the boundary layer. Bilgram has concluded that for the ice-water interface the boundary layer is between 1.4 and 6 μm thick. For the salol-melt interface, Durig has concluded that the boundary layer is about 1 μm thick. The boundary layer has properties distinct from those of the bulk fluid phase. Indirect support is provided by computer simulation experiments by Landman et al.[2] which show that a stratified structure develops in the melt adjacent to the growing surface of a crystal.

(5) Induced layer of liquid-crystal. In an earlier work[11] we sug-

gested that the interface of the growing crystal could induce orientational ordering in the molecules close to the interface, since the molecules to be attached to the crystal must have the "right" orientation. The behaviour of the boundary layer would be the behaviour of a nematic liquid-crystal near the nematic-isotropic phase transition, which possesses slowly relaxing collective modes[56] which scale with q^2. Scattering from these modes is generally much stronger than scattering from the isotropic fluid. However, recently we observed the same relaxational scattering when the crystal was melting. This observation weakens the liquid-crystal model since when the crystal is melting there is no necessity for orientational ordering of the molecules above the interface, though it might still be present.

Most theories of crystal growth are based on the assumption that the interface between crystal and melt is sharp or at most of the order of few atomic spacings. Landman's[2] computer simulation shows a stratified boundary layer of only a few atomic spacings. Therefore, it is important to perform additional experiments in which the boundary layer thickness could be measured directly.

If one considers a typical concentration of screw dislocations of the order of $10^3/cm^2$ and w/h of about 100, this would be enough to cause an "undulation" on the crystal surface of about 1 μm in height. Thus, a very thin boundary layer would nevertheless have an effective thickness of ~ 1 μm, in agreement with the results of Durig. On the other hand, since at our working angles for growth along the b direction the penetration depth of the evanescent wave is of the order of 800 Å, we would then expect to observe relaxa-

tional scattering in the geometry of Fig. 6.1a. The fact that no such scattering was observed makes it highly improbable that the boundary layer is much thinner than one μm.

CONCLUSIONS

Quasielastic laser light scattering performed at the crystal-melt interface of Salol revealed that two different dynamical processes are occurring simultaneously on the interface. These dynamical processes can be studied independently by proper choice of the scattering geometry. One dynamical process manifests itself by an oscillatory intensity autocorrelation function (oscillatory scattering) and we showed that it occurs at the crystal surface. The other dynamical process manifests itself by a relaxational intensity autocorrelation function (relaxational scattering) and we showed that it occurs in a thin boundary layer between the crystal surface and the bulk melt. This relaxational scattering was also observed when the crystal was melting.

From the analysis of the oscillatory scattering we concluded that the scattered light is Bragg diffracted and Doppler-shifted by the ledges of polygonized spirals originating at screw dislocations. The lateral velocity v_L of the steps was obtained from the frequency of the oscillatory autocorrelation function using the Doppler-shift equation. From the functional dependence of v_L vs. v_G (the growth velocity of the crystal), the mechanism of growth was determined without reference to the undercooling of the interface.

The temperature of the interface T_i was obtained by computer fitting of the thermistor readings to the solution of the heat-flow equation, taking into account the latent heat liberated at the interface and the heat transfer by convection with the ambient

air. From the analysis of v_L and v_G vs. T_i we obtained the kinetic coefficient for screw dislocation mediated growth by two different approaches. The values for the kinetic coefficient were self-consistent and in agreement with literature values obtained with traditional techniques in crystal growth. The morphology of the spirals was also determined and the parameters obtained from the experiment are in agreement with the values predict by the theory of spiral growth.

Several mechanisms were considered and discussed in attempting to explain the boundary layer dynamics. However, a consistent physical model has not yet been achieved. A computer simulation by Landman et al. indicates a stratified melt close to the interface extending a few atomic distances. Indirect estimates of the thickness of the boundary layer by Bilgram's group give values in the micrometer range. Therefore experiments where the thickness of the boundary layer could be measured directly are important to set the spatial scale of the phenomenon necessary for comparison with realistic physical models. Also experiments on low Jackson α-factor materials could indicate if there is any correlation between the boundary layer dynamics and the structure of the interface. It would also be interesting to perform additional experiments on materials with high melt viscosity to see if there is any correlation between the relaxation rate of the boundary layer dynamics and the viscosity of the melt.

This new field of quasielastic laser light scattering applied to the dynamics of crystal growth pioneered by Professor J.H.Bilgram has opened very exciting possibilities in crystal growth stu-

dies. It would be very interesting if we could observe and study the roughening transition in crystal surfaces with light scattering, or if we could observe and study with light scattering the slowing-down of the relaxation rate of the dynamical height fluctuations on the surface of crystals close to the Mullins-Sekerka instability . These experiments would provide accurate and detailed data necessary for comparison with the great amount of recent theoretical work on the dynamics of crystal growth, and would hopefully improve our understanding about critical phenomena and pattern selection in nature.

APPENDIX A

Heat flow problem in our apparatus

Considering the apparatus illustrated in Figure 5.2, let us name the parameters involved :

a_1 = radius of the tube containing the crystal ;

a_2 = radius of the plexiglas cylinder ;

b = height of the plexiglas cylinder;

zi = position of the interface in relation to the lower aluminum cylinder ;

h = convective heat transfer coefficient ;

TU = temperature of the upper aluminum cylinder ;

TL = temperature of the lower aluminum cylinder ;

TA = temperature of the circulating air around the plexiglas cylinder ;

L = latent heat of fusion = 27.2 cal cm^{-3} [57];

v_G = growth velocity of the crystal ;

k = thermal conductivity of the plexiglas, Salol melt and Salol solid, assumed to be the same in this approximation.

The literature values for the thermal conductivities are :

a) for liquid Salol

$k = 1.80 \times 10^4$ erg $cm^{-1}s^{-1}K^{-1}$ [58]

$k = 1.35 \times 10^4$ erg $cm^{-1}s^{-1}K^{-1}$ [59]

b) for solid Salol

$k = 2.51 \times 10^4$ erg $cm^{-1}s^{-1}K^{-1}$ [58]

c) for the plexiglas

$k = 1.70 \times 10^4$ erg $cm^{-1}s^{-1}K^{-1}$ [60].

In our calculations we used the thermal conductivity of the plexiglas.

The fits of the thermistors readings to the theoretical expression which we are going to derive below are very good. Also the melting temperatures obtained from the fits are in good agreement with known values, indicating that the error introduced by considering equal thermal conductivities is not large.

The system has azimuthal symmetry and the temperature profile is measured when the interface of the crystal reaches the steady-state situation. Thus we have to solve the Laplace equation

$$\nabla^2 T(r,z) = 0$$

with the following boundary conditions :

$$T(r,b) = TU$$

$$T(r,0) = TL$$

$$T(r,zi+) = T(r,zi-)$$

where zi+ and zi- are the positions of the melt and crystal sides of the interface,

$$-k\frac{\partial T}{\partial r})a_2 = h\,[T(a_2,z)-TA]$$

which is Newton's law for convective heat exchange,

$$\frac{H(a_1-r)v_G L}{k} = \frac{\partial T}{\partial z})zi+ - \frac{\partial T}{\partial z})zi-$$

which is the boundary condition related to the heat conservation at the interface. $H(a_1-r)$ is the Heavyside function whose values in this case are 1 for $r<a_1$ and 0 for $r>a_1$.

It is convenient to make the following variable change

$$\theta(r,z) = T(r,z) - TA \tag{A1}$$

and rewrite the previous equations

$$\nabla^2\theta(r,z) = 0 \tag{A2}$$

$$\theta(r,b) = TU-TA \tag{A3}$$

$$\theta(r,0) = TL-TA \tag{A4}$$

$$\theta(r,zi+) = \theta(r,zi-) \tag{A5}$$

$$-k\frac{\partial\theta}{\partial r})a_2 = h\theta(a_2,z) \tag{A6}$$

$$\frac{H(a_1-r)v_G L}{k} = \frac{\partial\theta}{\partial z})zi+ - \frac{\partial\theta}{\partial z})zi- \tag{A7}$$

Writing (A2) in cylindrical coordinates and making use of the azimuthal symmetry we obtain

$$(\frac{1}{r})\frac{\partial}{\partial r}(\frac{r\partial\theta}{\partial r}) + \frac{\partial^2\theta}{\partial^2 z} = 0$$

If we write $\theta(r,z) = R(r)Z(z)$ we can separate the above equation into two equations, namely

$$\frac{d^2Z}{dz^2} - \lambda_n^2 Z = 0$$

whose solution is

$$Z(z) = A_n\cosh(\lambda_n z) + B_n\sinh(\lambda_n) \qquad \text{and}$$

$$\frac{d^2R}{dr^2} + (\frac{1}{r})\frac{dR}{dr} + \lambda_n^2 R = 0$$

whose solution is

$$R(r) = C_n\, J_o(\lambda_n r) + D_n\, N_o(\lambda_n r)$$

where the λ_n are determined from the boundary conditions and J_o and N_o are the zero order Bessel and Neumman functions respectively. Since we are interested in the temperature profile inside of the chamber, N_o cannot be a solution to the problem since it diverges at the origin. So the complete solution can be written as,

$$\theta(r,z) = \sum_{\lambda_n} J_0(\lambda_n r)[A_n \cosh(\lambda_n r) + B_n \sinh(\lambda_n r)] \tag{A8}$$

By applying boundary condition (A6) we obtain,

$$\sum_{\lambda_n} \lambda_n J_1(\lambda_n a_2)[A_n \cosh(\lambda_n z) + B_n \sinh(\lambda_n z)] =$$

$$\frac{h}{k} \sum_{\lambda_n} J_0(\lambda_n a_2)[A_n \cosh(\lambda_n z) + B_n \sinh(\lambda_n z)]$$

which implies for every λ_n,

$$\lambda_n J_1(\lambda_n a_2) = \frac{h}{k} J_0(\lambda_n a_2) \quad .$$

Let us further call $\lambda_n a_2 = \delta_n$ and $\frac{h a_2}{k} = P$, then

$$\delta_n J_1(\delta_n) = P J_0(\delta_n) \tag{A9}$$

Before proceeding it is useful to derive some mathematical expressions involving the Bessel functions. From the theory of Bessel functions we have, for a different than b,

$$\int x J_p(ax) J_p(bx) dx = \left(\frac{1}{a^2 - b^2}\right)[bx J_p(ax) J_{p-1}(bx) - ax J_{p-1}(ax) J_p(bx)]$$

Thus for δ_n different than δ_m where the deltas are given by (A9), we have

$$\int_0^{a_2} r J_0\left(\frac{\delta_n r}{a_2}\right) J_0\left(\frac{\delta_m r}{a_2}\right) dr = 0 \quad .$$

For a = b,

$$\int x[J_p(ax)]^2dx = \frac{x^2}{2}\left[[J_p(ax)]^2 - J_{p-1}(ax)J_{p+1}(ax)\right] .$$

Thus for δ_n equal δ_m, we obtain,

$$\int_0^{a_2} rJ_0^2(\frac{\delta_n r}{a_2})dr = \frac{a_2}{2}[J_0^2(\delta_n)+J_1^2(\delta_n)]$$

To summarize the previous results we can write ,

$$\int_0^{a_2} rJ_0(\frac{\delta_n r}{a_2})J_0(\frac{\delta_m r}{a_2})dr = \frac{a_2^2}{2}[J_0^2(\delta_n)+J_1^2(\delta_n)]\delta_{\delta_n\delta_m} \qquad (A10)$$

Therefore to expand an arbitrary function in terms of $J_0(\frac{\delta_n r}{a_2})$, namely

$$f(r) = \sum_{\delta_n}^{\infty} C_n J_0(\frac{\delta_n r}{a_2})$$

C_n will be given by ,

$$C_n = \frac{2}{a_2^2[J_0^2(\delta_n)+J_1^2(\delta_n)]}\int_0^{a_2} rf(r)J_0(\frac{\delta_n r}{a_2})dr \qquad (A11)$$

In particular if f(r) = K constant and using the expression

$$\int_0^{a_2} rJ_0(\frac{\delta_n r}{a_2})dr = \frac{a_2^2 J_1(\delta_n)}{\delta_n}$$

the expression (A11) can be written as ,

$$C_n = \frac{2KJ_1(\delta_n)}{\delta_n[J_0^2(\delta_n)+J_1^2(\delta_n)]}$$

Finally, using (A9) we obtain,

$$C_n = \frac{2KP}{J_o(\delta n)[\delta n^2+P^2]} \tag{A12}$$

Since there are two different media, liquid and solid, we have to consider the solutions in each medium and match the boundary conditions at the interface. Thus it is convenient to write the solutions as:

a) for z > zi (liquid side)

$$\theta_L = \sum_{\delta n}^{\infty} J_o(\frac{\delta n r}{a_2})\left[A_n\cosh(\frac{\delta n z}{a_2}) + B_n\sinh(\frac{\delta n z}{a_2})\right] \tag{A13}$$

b) for z < zi (solid side)

$$\theta_S = \sum_{\delta n}^{\infty} J_o(\frac{\delta n r}{a_2})\left[C_n\cosh(\frac{\delta n z}{a_2}) + D_n\sinh(\frac{\delta n z}{a_2})\right] \tag{A14}$$

The δ_n are the same for the two solutions since we assumed that all the thermal conductivities are equal and the convective heat transfer coefficient is uniform in the thermostat. Let us now apply the remainder boundary conditions. Using (A3) and (A13) we have,

$$TU-TA = \sum_{\delta n}^{\infty} J_o(\frac{\delta n r}{a_2})\left[A_n\cosh(\frac{\delta n b}{a_2}) + B_n\sinh(\frac{\delta n b}{a_2})\right] .$$

By using the expression (A12) we obtain,

$$A_n\cosh(\frac{\delta n b}{a_2}) + B_n\sinh(\frac{\delta n b}{a_2}) = \frac{2(TU-TA)P}{J_o(\delta n)[\delta n^2+P^2]} \tag{A15}$$

Using (A4), (A14) and (A12) we obtain,

$$C_n = \frac{2(TL-TA)P}{J_o(\delta n)[\delta n^2+P^2]} \tag{A16}$$

Using (A5), (A13) and (A14) we obtain,

$$A_n\cosh(\frac{\delta_n z_i}{a_2}) + B_n\sinh(\frac{\delta_n z_i}{a_2}) = C_n\cosh(\frac{\delta_n z_i}{a_2}) + D_n\sinh(\frac{\delta_n z_i}{a_2}) \qquad (A17)$$

By using (A7), (A13), (A14) and (A11) we obtain,

$$(C_n-A_n)\sinh(\frac{\delta_n z_i}{a_2}) + (D_n-B_n)\cosh(\frac{\delta_n z_i}{a_2}) = \frac{2v_G L a_1}{k}\frac{J_1(\frac{\delta_n a_1}{a_2})}{[J_o(\delta_n)]^2(\delta_n^2+P^2)} \qquad (A18)$$

Equations (A15), (A16), (A17) and (A18) form a set of 4 equations and 4 unknowns. Therefore A_n, B_n, C_n and D_n can be determined. If we write

$$\beta_n = \frac{2P}{J_o(\delta_n)[\delta_n^2+P^2]} \qquad \text{and}$$

$$\gamma_n = \frac{v_G L a_1}{Pk}\frac{J_1(\frac{\delta_n a_1}{a_2})}{J_o(\delta_n)}$$

the final solutions are :

a) for z > zi (liquid side)

$$T_L(r,z) = TA + \sum_{\delta_n}^{\infty} \beta_n J_o(\frac{\delta_n r}{a_2})[(TL-TA)\left[\cosh(\frac{\delta_n z}{a_2}) - \coth(\frac{\delta_n b}{a_2})\sinh(\frac{\delta_n z}{a_2})\right] + \frac{(TU-TA)\sinh(\frac{\delta_n z}{a_2})}{\sinh(\frac{\delta_n b}{a_2})} + \gamma_n\sinh(\frac{\delta_n z_i}{a_2})\left[\cosh(\frac{\delta_n z}{a_2}) - \coth(\frac{\delta_n b}{a_2})\sinh(\frac{\delta_n z}{a_2})\right]] \qquad (A19)$$

b) for z < zi (solid side)

$$T_S(r,z) = TA + \sum_{\delta_n}^{\infty} \beta_n J_0\left(\frac{\delta_n r}{a_2}\right)\left[(TL-TA)\left[\cosh\left(\frac{\delta_n z}{a_2}\right) - \coth\left(\frac{\delta_n b}{a_2}\right)\sinh\left(\frac{\delta_n z}{a_2}\right)\right] + \frac{(TU-TA)\sinh\left(\frac{\delta_n z}{a_2}\right)}{\sinh\left(\frac{\delta_n b}{a_2}\right)} + \gamma_n \sinh\left(\frac{\delta_n z}{a_2}\right)\left[\cosh\left(\frac{\delta_n zi}{a_2}\right) - \coth\left(\frac{\delta_n zi}{a_2}\right)\sinh\left(\frac{\delta_n zi}{a_2}\right)\right]\right] \qquad (A20)$$

We fit the thermistor readings to expressions (A19) and (A20) at fixed r = 1.27 cm (corresponding to the position of the thermistors embedded in the plexiglas cylinder). TU, TA, TL, and P were free parameters in the fit. For each value of P the δ_n were calculated using equation (A9). The parameters TU, TA, TL, and P were obtained from the best-fit values. Subsequently, they were used in expressions (A19) and (A20) with z = zi (position of the interface measured by the traveling microscope) to calculate the temperature of the interface as a function of r. T_i is the temperature at the center of the interface (at r = 0) where the laser beam intersects the interface. By numerically differentiating eqs. (A19) and (A20) the temperature gradient normal to the interface at r = 0 was also obtained for both the liquid and solid sides.

REFERENCES

1. H.A.Wilson, Phil. Mag. 50, 238 (1900).
2. U.Landman, C.L.Cleveland, C.S.Brown, and R.N.Barnett, in: Nonlinear Phenomena at Phase Transitions and Instabilities, ed. T.Riste, Plenum Press, New York (1983), p. 379.
3. J.Q.Broughton and G.H.Gilmer, to be published.
4. J.H.Bilgram, H.Guttinger, and W.Kanzig, Phys. Rev. Lett. 40, 1394 (1978).
5. H.Guttinger, J.H.Bilgram, and W.Kanzig, J. Phys. Chem. Solids 40, 55 (1979).
6. J.H.Bilgram and P.Boni, in: Light Scattering in Liquids and Macromolecular Solutions, ed. V.DeGiorgio, M.Corti, and M.Giglio, Plenum Press, New York (1980), p. 203.
7. P.Boni, J.H.Bilgram, and W.Kanzig, Phys. Rev. A 28, 2953 (1983).
8. U.Durig and J.H.Bilgram, in: Nonlinear Phenomena at Phase Transitions and Instabilities, ed. T.Riste, Plenum Press, New York (1982), p. 371.
9. U.Durig, Ph.D. Thesis, E.T.H., Zurich (1984).
10. R.A.Brown, J.Keizer, U.Steiger, and Y.Yeh, J. Phys. Chem. 87, 4135 (1983).
11. O.N.Mesquita, D.G.Neal, M.Copic, and H.Z.Cummins, Phys. Rev. B 29, 2846 (1984).
12. W.K.Burton, N.Cabrera, and C.Frank, Phil. Trans. R. Soc. London, Ser. A243, 299 (1951).
13. K.A.Jackson, in: Liquid Metals and Solidification, American Society

for Metals, Cleveland, Ohio (1958), p. 174

14. K.A.Jackson, in: Crystal Growth a Tutorial Approach, ed. J.B.Mullin, D.T.J.Hurle, and W.Bardsley, North-Holland Pub., Amsterdam (1979), p. 139.

15. J.D.Weeks and G.H.Gilmer, in: Advances in Chemical Physics, ed. I.Prigogine and S.A.Rice, John Wiley & Sons, New York (1979), vol. 40, p. 157.

16. W.W.Mullins and R.F.Sekerka, J. Appl. Phys. 34, 323 (1963); 35, 444 (1964).

17. J.S.Langer, Rev. Mod. Phys. 52, 1 (1980).

18. M.Kerszberg, Phys. Rev. B 27, 3909 (1983).

19. M.E.Gliksman, R.J.Schaefer, and J.D.Ayers, Metall. Trans.A 7A, 1747 (1976).

20. J.Frenkel, Physik Z. Sov. 1, 498 (1932).

21. K.A.Jackson, in: Crystal Growth and Characterization, ed. R.Ueda and J.B.Mullin, North-Holland Pub., Amsterdam (1975), p. 21.

22. F.C.Frank, Disc. Faraday Soc. 5, 48 (1949).

23. L.J.Griffin, Phil. Mag. 41, 196 (1950).

24. A.R.Verma, Crystal Growth and Dislocations, Academic Press Inc., New York (1953).

25. A.J.Forty, Phil. Mag. 43, 377 (1952).

26. G.W.Sears, J. Chem. Phys. 23, 1630 (1955).

27. I.Sunagawa and P.Bennema, in: Preparation and Properties of Solid State Materials, ed. W.R.Wilcox, Marcel Dekker Inc., New York (1982), vol. 7.

28. P.Cladis, private communication.

29. K.A.Jackson, in: Surface Modification and Alloying, ed. J.M.Poate,

G.Foti, and D.C.Jacobson, Plenum Pub. Corp., New York (1983), p.51.

30. K.A.Jackson and C.E.Miller, J. Crystal Growth 40, 169 (1977).

31. J.E.Avron, L.S.Balfour, C.G.Kuper, J.Landau, S.G.Lipson, and L.S.Schulman, Phys. Rev. Lett. 45, 814 (1980).

32. J.E.Hilliard and J.W.Cahn, Acta Metal. 6, 772 (1958).

33. J.W.Cahn, W.B.Hillig, and G.W.Sears, Acta Metal. 12, 1421 (1964).

34. K.A.Jackson, D.R.Uhlmann, and J.D.Hunt, J. Crystal Growth 1, 1 (1967).

35. T.H.Ie and R.F.Strickland-Constable, J. Crystal Growth 21, 243 (1974)

36. D.E.Ovsienko and G.A.Alfintsev, in: Crystals, Growth, Properties and Applications, ed. H.C.Freyhardt, Springer-Verlag, Berlin (1980), p. 119

37. S.Tolanski, Multiple Beam Interferometry, Oxford University Press, London (1948).

38. Yu.S.Kaganovskii and A.A.Onoprienko, Sov. Phys. Solid State 20, 1335 (1978).

39. K.Tsukamoto, J. Crystal Growth 61,199 (1983).

40. A.T.Forrester, R.A.Gudmundsen, and P.O.Johnson, Phys. Rev. 99, 1691 (1955).

41. A.T.Forrester, J. Opt. Soc. Am. 51, 253 (1961).

42. H.Z.Cummins and H.L.Swinney, in: Progress in Optics, ed. E.Wolf, North-Holland Pub., Amsterdam (1970), vol. 8, p. 133.

43. Photon Correlation and Light Beating Spectroscopy, ed. H.Z.Cummins and E.R.Pike, Nato Advanced Study Institute Series, Plenum Press, New York (1974).

44. H.Z.Cummins, N.Knable, L.Gampel, and Y.Yeh, Appl. Phys. Lett. 2, 62

(1963).

45. D.P.Woodruff, The Solid-Liquid Interface, Cambridge University Press, London (1973).

46. R.F.Strickland-Constable, Kinetics and Mechanics of Crystallization, Academic Press, London (1968).

47. K.A.Jackson, in: Treatise on Solid State Chemistry, ed. N.B.Hannay, Plenum Press, New York (1975), vol. 5, p. 233.

48. W.B.Hillig and D.Turnbull, J. Chem. Phys. 24, 914 (1956).

49. K.A.Jackson and J.D.Hunt, Acta Metal. 13, 1212 (1965).

50. I.Flachsbart, Naturwissenschaften 44, 348 (1957).

51. J.H.Bilgram, U.Durig, M.Wachter, and P.Seiler, J. Crystal Growth 57, 1 (1982).

52. M.A.Awal, Ph.D. Thesis, City College of the City University of New York, New York (1983).

53. O.Jantsch, Z. Kristallogr. 108, 185 (1956).

54. D.Turnbull, J. Appl. Phys. 21, 1022 (1950).

55. P. Di Porto, B.Crosignani, and M.Bertolotti, J. Appl. Phys. 40, 5083 (1969).

56. C.f. Orsay Liquid Crystal Group, Phys. Rev. Lett. 22, 1361 (1969)

57. H.Pollatschek, Z. Phys. Chem. A142, 289 (1929).

58. K.Neumann and D.M. Al Yawir, J. Crystal Growth 11, 323 (1971).

59. L.P.Filippov, Chem. Abstracts 56, 10936a (1962).

60. CRC Handbook of Chemistry and Physics, ed. R.C.Weast and M.J.Astle, CRC Press Inc., Florida (1979-1980), 60th. edition.

FIGURE CAPTIONS

Fig. 4.1 - Morphology of a typical Salol crystal grown from solution, showing prominent growth faces.

Fig. 4.2 - Crystal-growth apparatus used in step 2 of the sample preparation procedure to grow the starting Salol crystals by the Bridgman technique.

Fig. 4.3 a) - Apparatus used in step 3 to remove the starting crystal from the growth tube, and used in step 8 to shift the main crystal for zone refining.

Fig. 4.3 b) - Apparatus used in step 8 of the sample preparation procedure to zone refine the seed and the crystal.

Fig. 5.1 - Overall layout of the crystal-melt spectrometer.

Fig. 5.2 - Crystal-growth thermostat. ACU - Upper aluminum cylinder, TU ~ 43.5°C; ACL - Lower aluminum cylinder, TL ~ 35.5°C; PC - Plexiglas cylinder; GS - Glass sleeve; AS - Air space, TA ~ 39.5°C; RS - Rotary stage; S - Teflon stopcock; L - Incident laser beam; TH - Thermistors.

Fig. 6.1 - Scattering geometries.

Fig. 6.2 - Correlation function of light scattered from the growing crystal surface observed in the geometry of Fig. 6.1a in VT polarization. ($\theta = 45^{\circ}$; $v_G = 0.20$ μm/s). The circles are the experimental data. The solid line is a computer fit giving $f = 61.89$ Hz and $v_L = 21.8$ μm/s.

Fig. 6.3 - Correlation function of light scattered from the fluid boundary layer observed in the geometry of Fig. 6.1b in HT polarization. The circles are the experimental data. The solid line is a computer fit giving $\Gamma^{-1} = 26.9$ ms and $D = 0.76 \times 10^{-9}$ cm^2/s.

Fig. 7.1 - Frequency of the oscillatory correlation function of the scattered light as a function of $\sin(\theta/2)$ for fixed angle of incidence ψ. The circles are the experimental data. The straight line is the prediction of the Doppler-shift equation.

Fig. 7.2 - Vertical temperature profile of the thermostat shown in Fig. 5.2 . The circles are the thermistors readings. The solid line is a computer fit to the heat flow equations derived in Appendix A.

Fig. 8.1 - Lateral velocity v_L vs. growth velocity v_G. Crosses are experimental points. The solid line is the prediction of the screw dislocation model (Eq. 8.3); the dashed line is the prediction of the surface nucleation model (Eq. 8.2).

Fig. 8.2 - Lateral velocity v_L vs. temperature of the interface

T_i. Circles are the experimental points. Solid line is the computer fit using Eq. 8.1 .

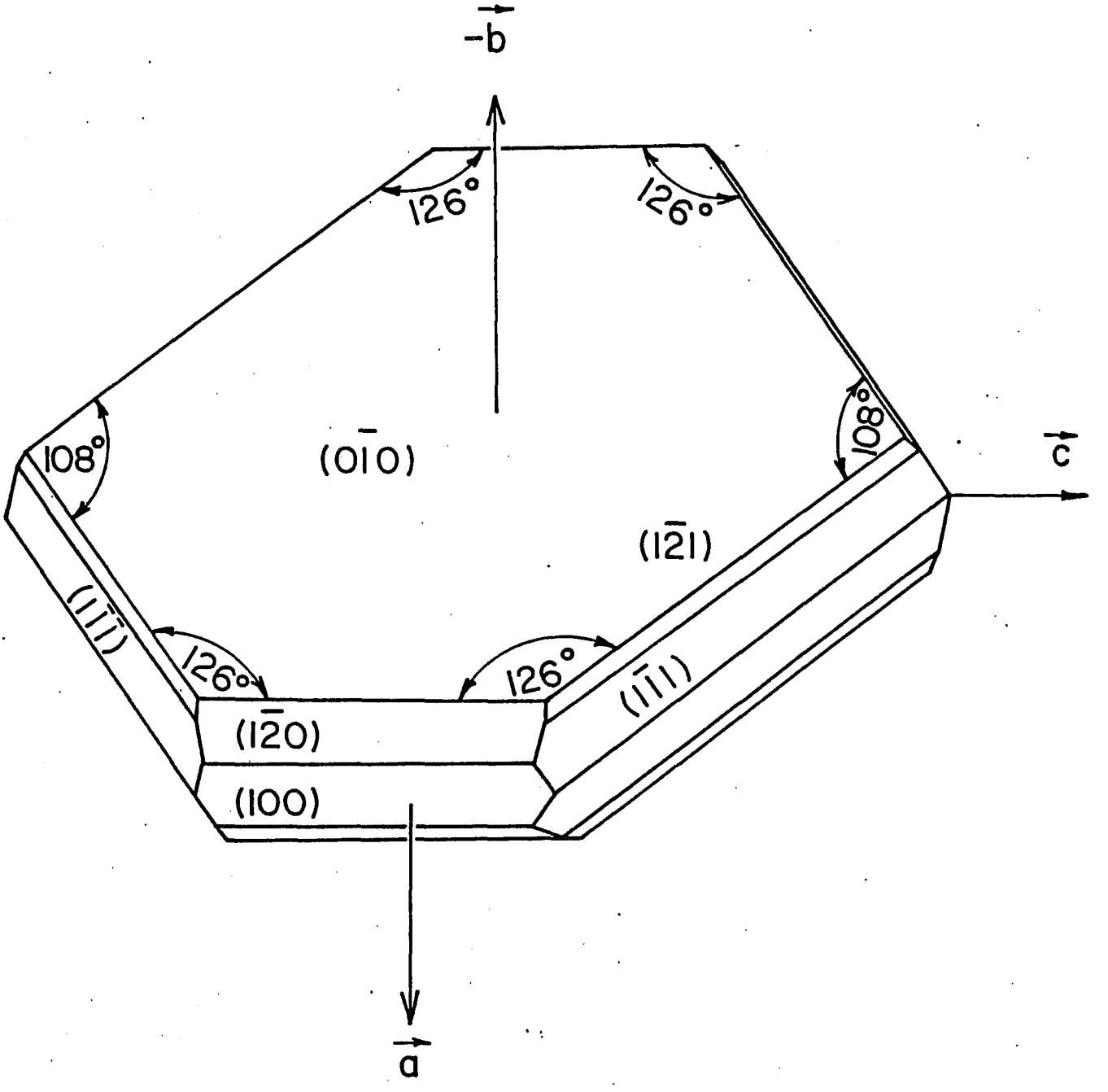
-b
126°
126°
108°
108°
(0$\bar{1}$0)
c
(1$\bar{2}$1)
(11$\bar{1}$)
126°
126°
(1$\bar{1}$1)
(1$\bar{2}$0)
(100)
a

4.1

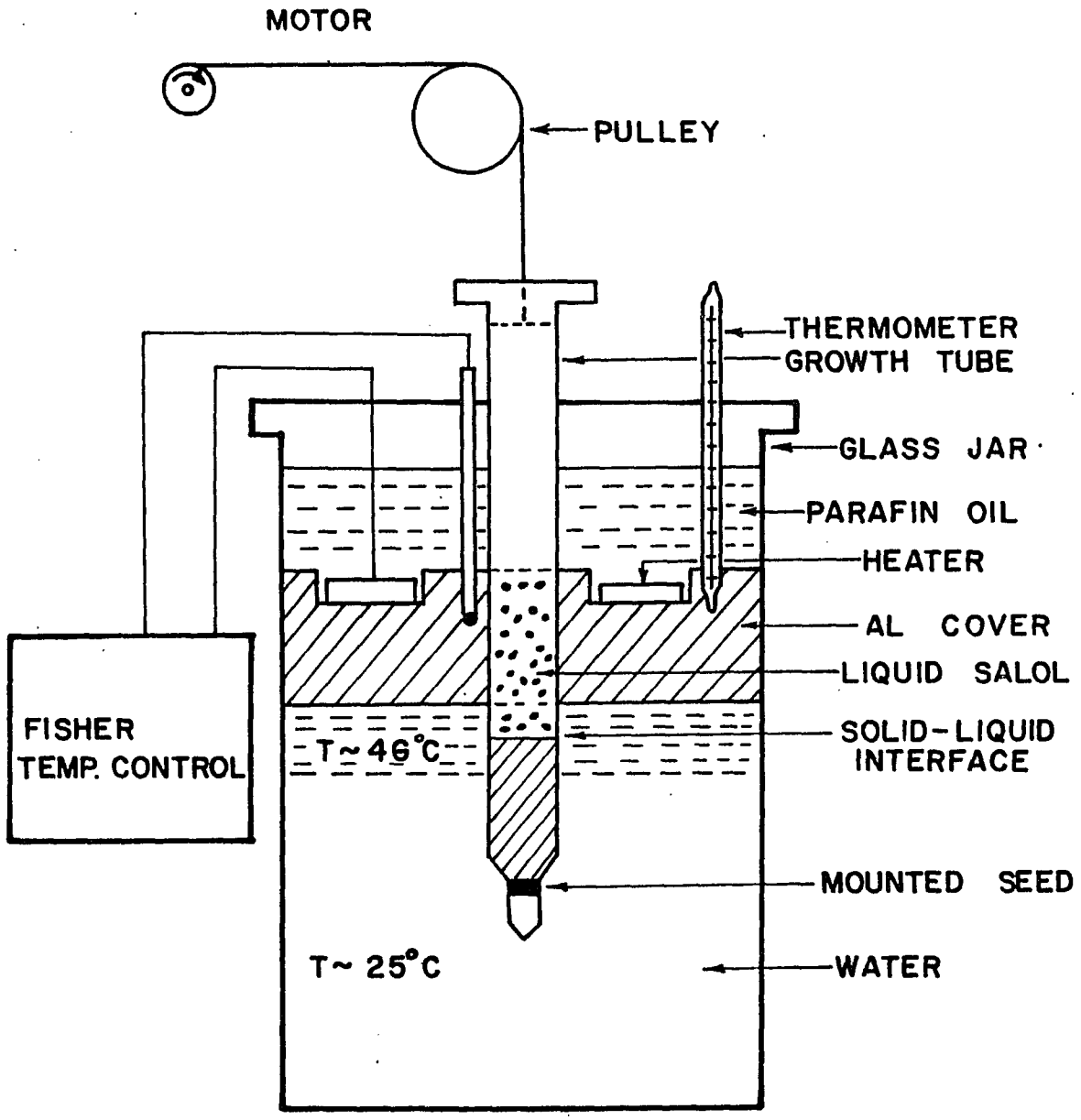
MOTOR
PULLEY
THERMOMETER
GROWTH TUBE
GLASS JAR
PARAFIN OIL
HEATER
AL COVER
LIQUID SALOL
SOLID-LIQUID INTERFACE
MOUNTED SEED
WATER
FISHER TEMP. CONTROL
T~ 46°C
T~ 25°C

4.2

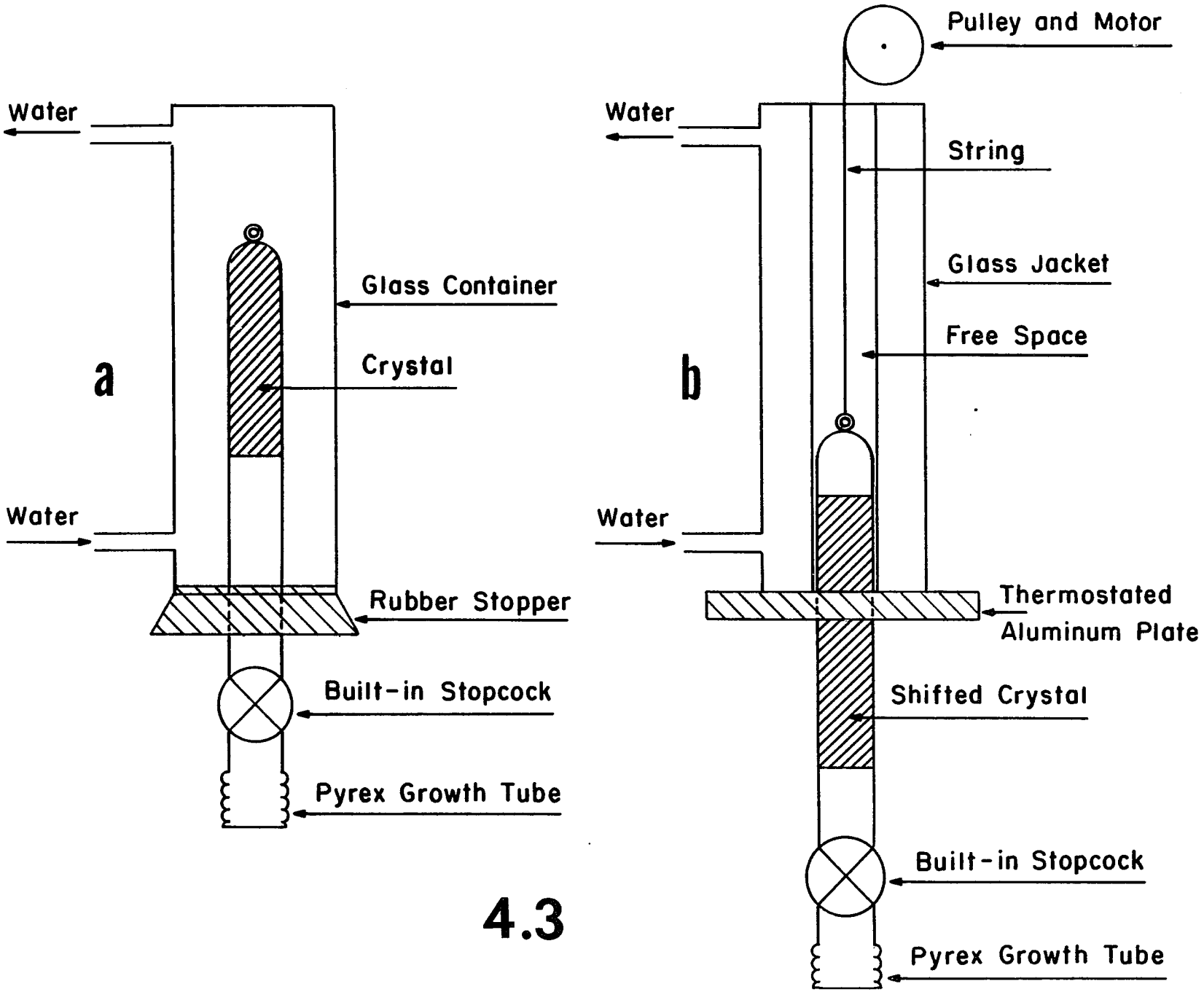
Water
Glass Container
a
Crystal
Water
Rubber Stopper
Built-in Stopcock
Pyrex Growth Tube
Pulley and Motor
Water
String
Glass Jacket
Free Space
b
Water
Thermostated
Aluminum Plate
Shifted Crystal
Built-in Stopcock
Pyrex Growth Tube

4.3

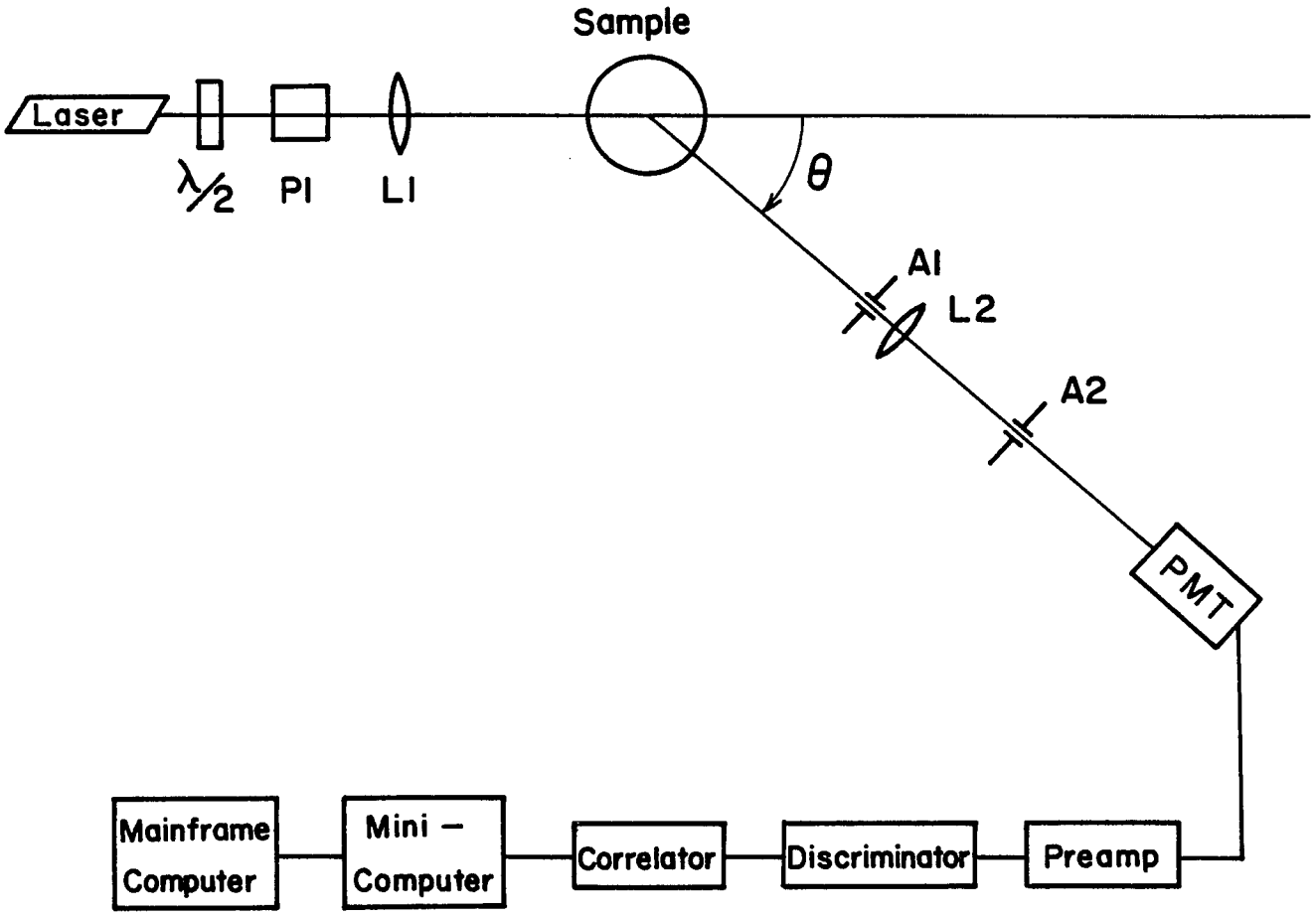
Sample
Laser
λ/2
PI
LI
θ
AI
L2
A2
PMT
Mainframe Computer
Mini – Computer
Correlator
Discriminator
Preamp

FIG. 5.1

5.1

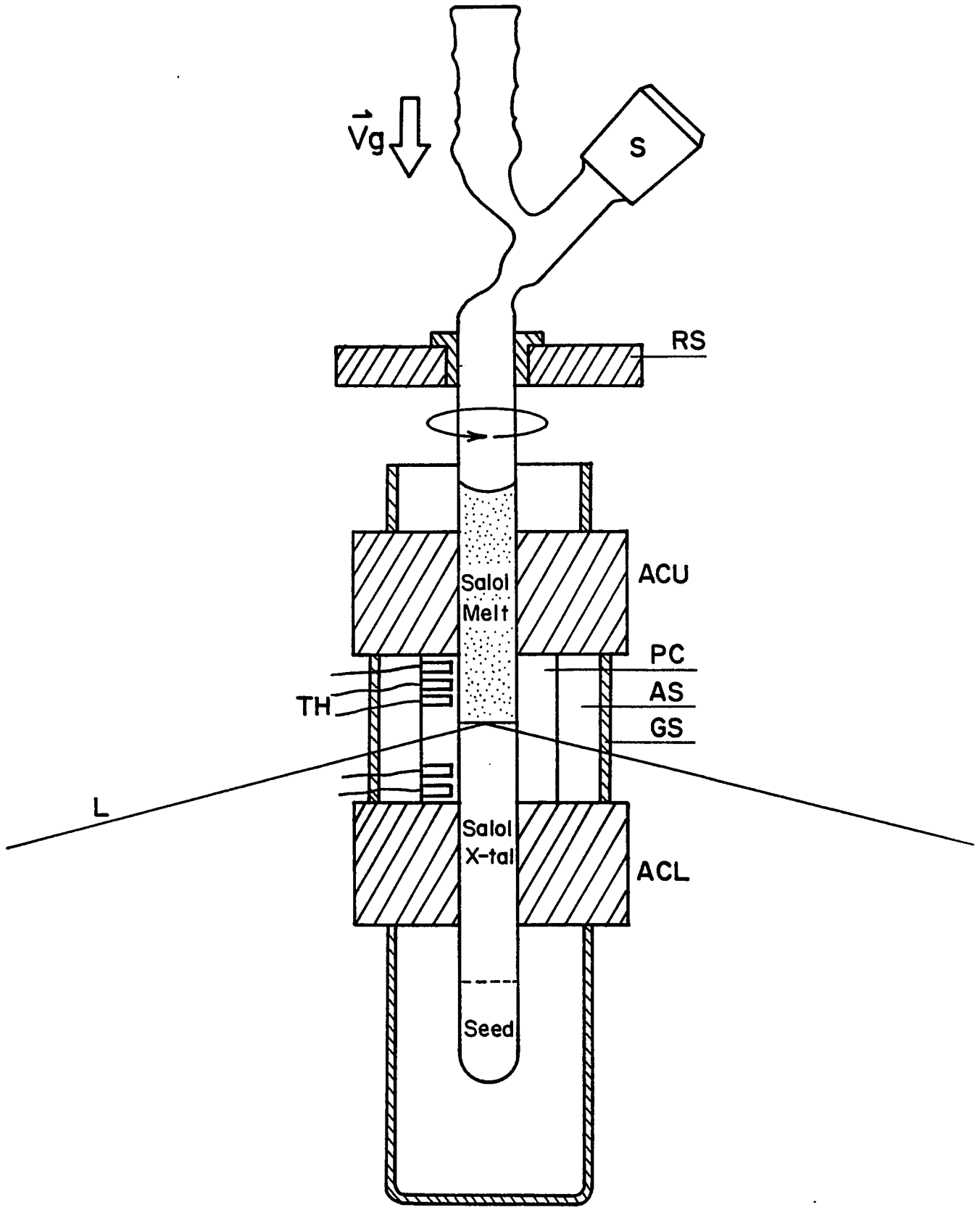

5.2

Scattering Geometries

a)

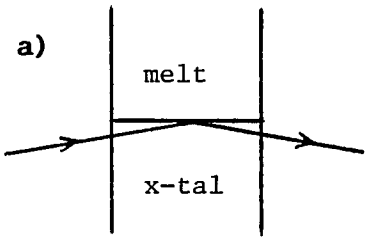

VT polarization

Beam totally internally reflected

Very anisotropic scattering

Oscillatory intensity autocorrelation function

b)

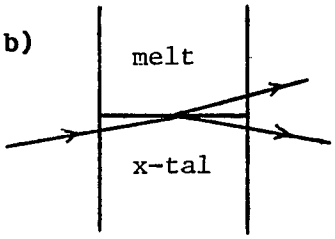

HT polarization

Beam partially transmitted

Relaxational intensity autocorrelation function

c)

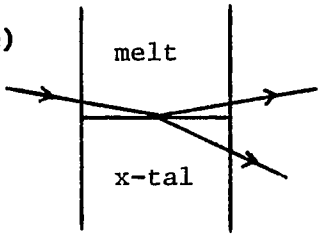

Any polarization

Relaxational intensity autocorrelation function

Scattering was observed when the crystal was either growing or melting

d)

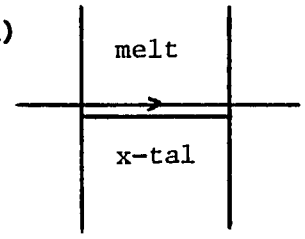

Weak scattering characteristic of the bulk melt

6.1

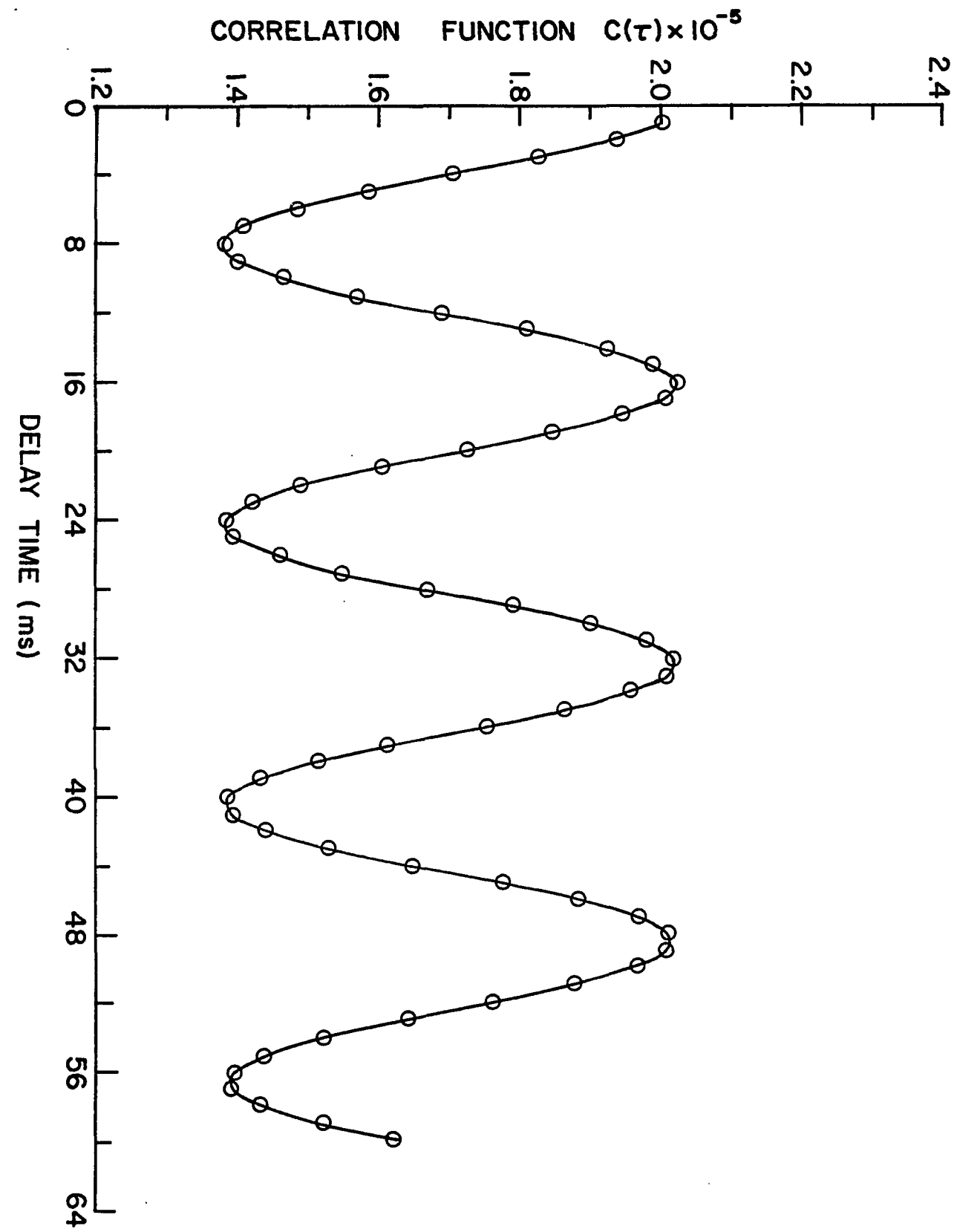
CORRELATION FUNCTION C(τ)×10⁻⁵
1.2
1.4
1.6
1.8
2.0
2.2
2.4
0
8
16
24
32
40
48
56
64
DELAY TIME (ms)

6.2

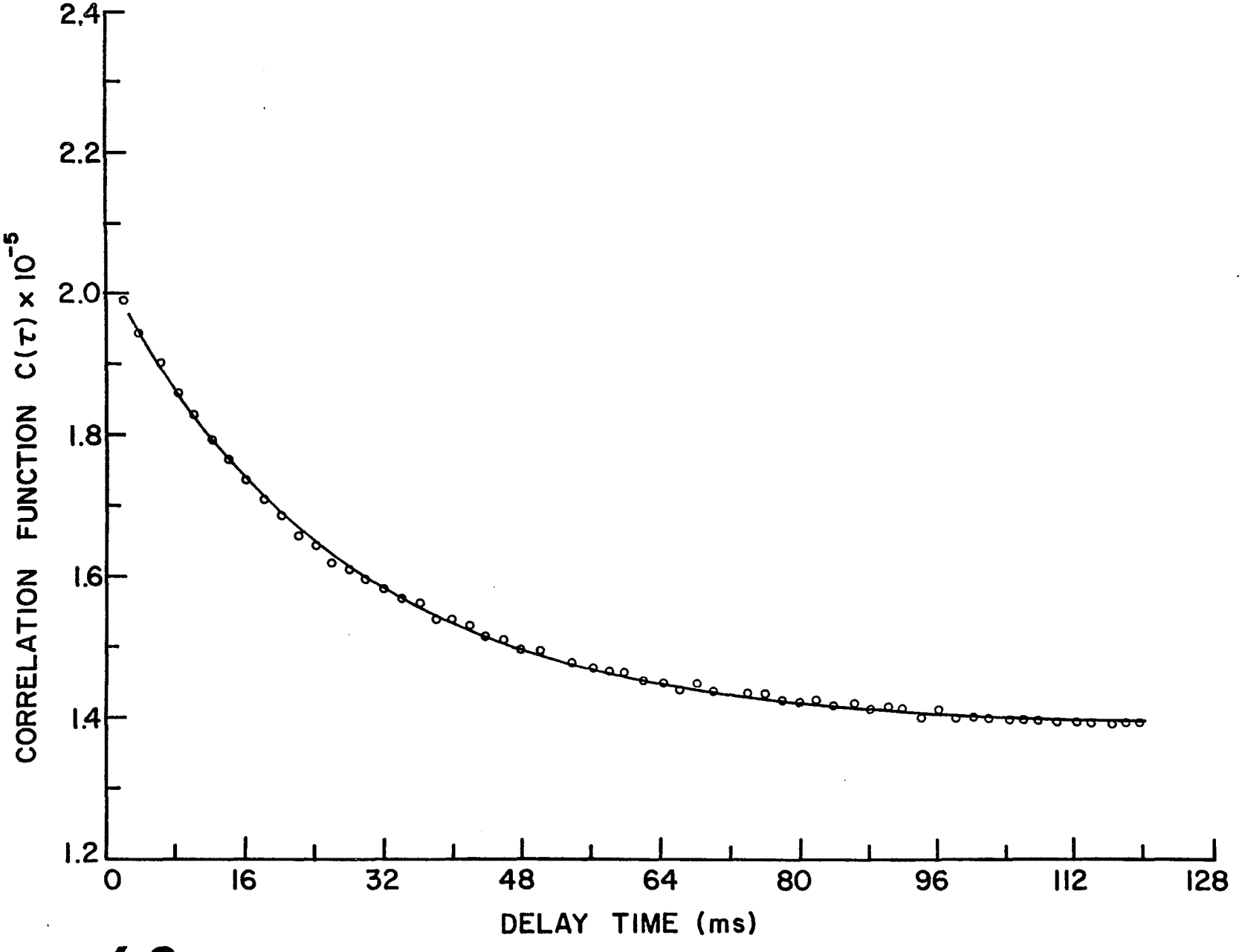
2.4
2.2
2.0
1.8
1.6
1.4
1.2
CORRELATION FUNCTION C(τ) x 10^-5
0
16
32
48
64
80
96
112
128
DELAY TIME (ms)

6.3

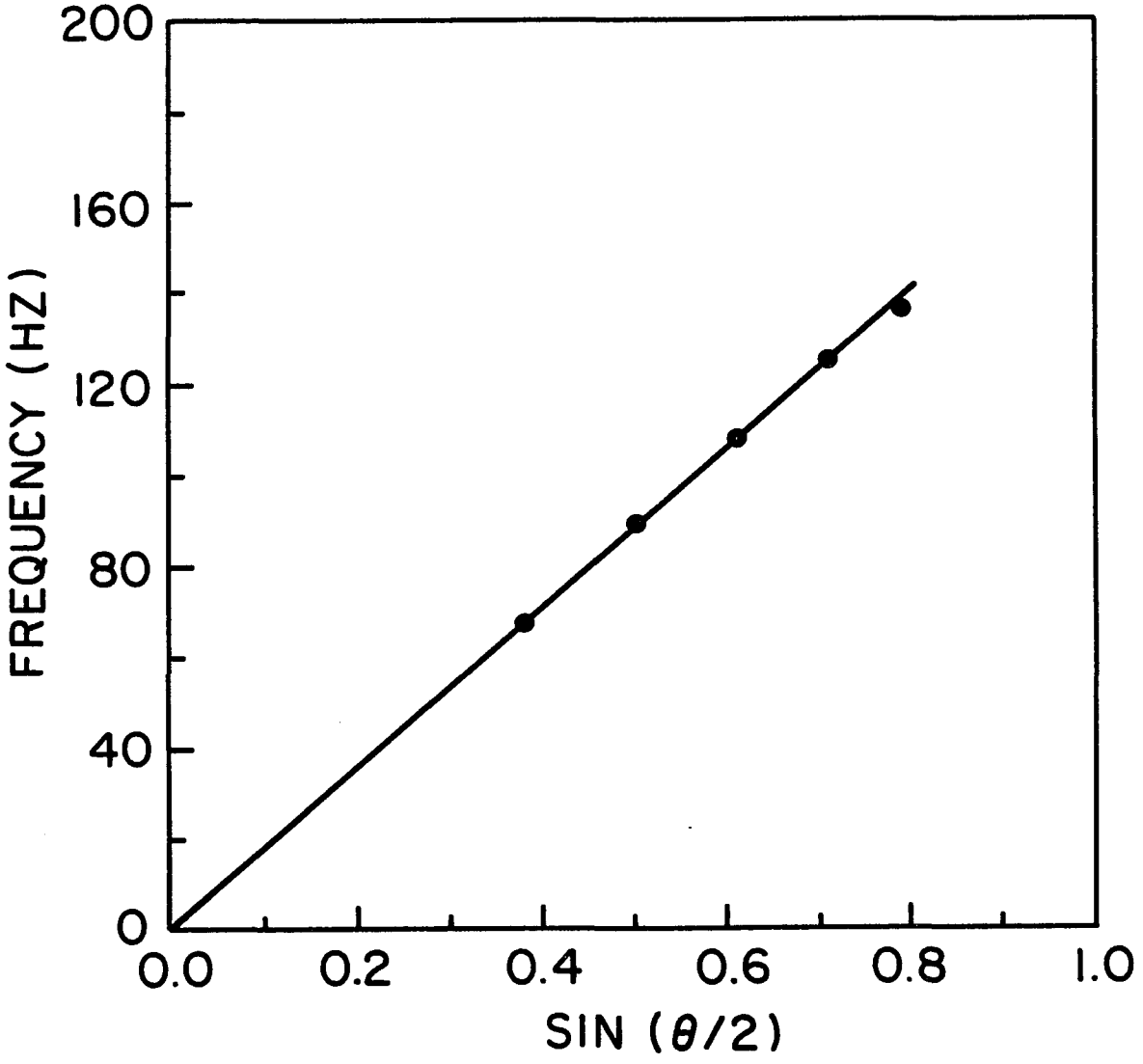

7.1

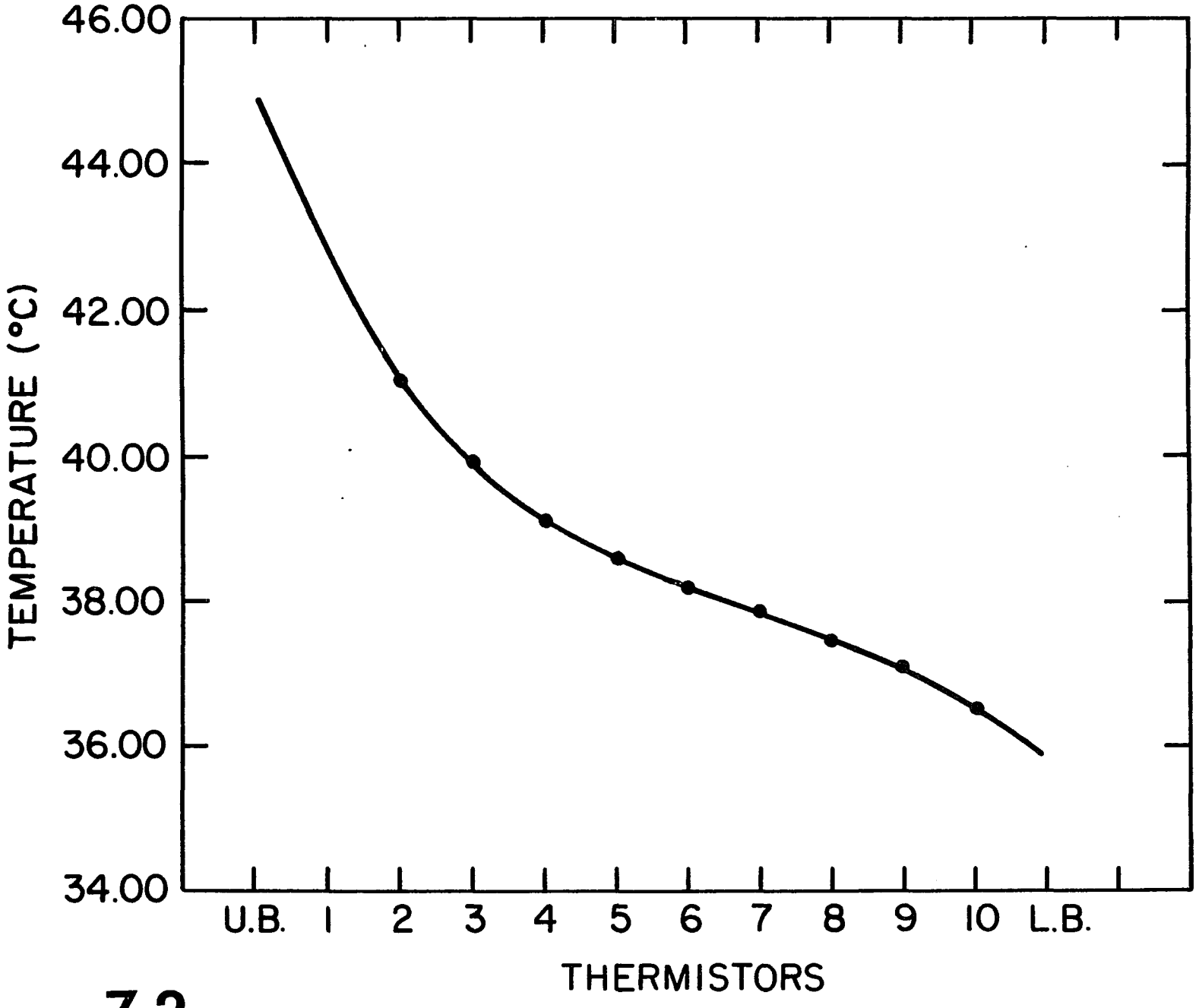
46.00
44.00
42.00
40.00
38.00
36.00
34.00
TEMPERATURE (°C)
U.B.
1
2
3
4
5
6
7
8
9
10
L.B.
THERMISTORS

7.2

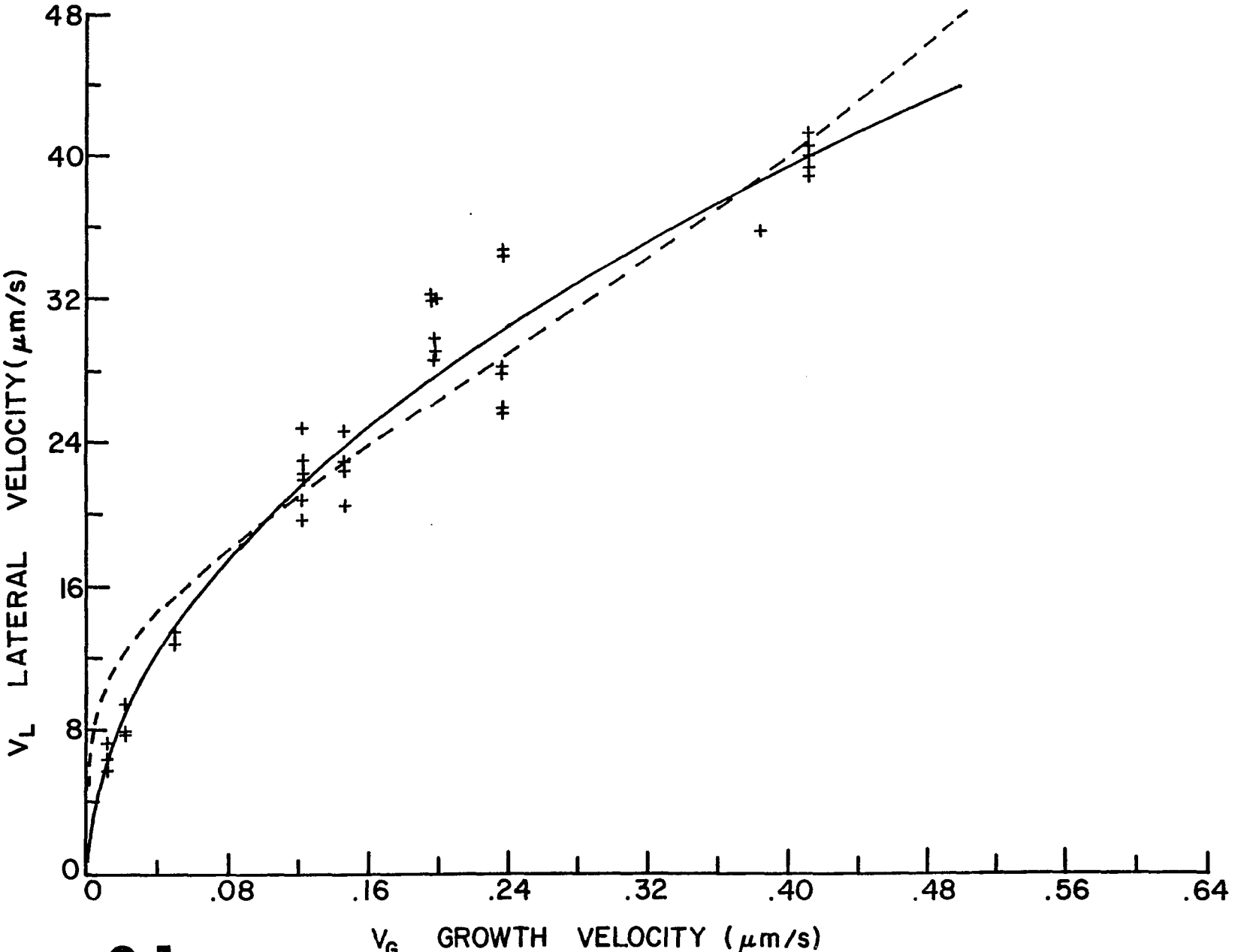
48
40
32
24
16
8
0
V_L LATERAL VELOCITY (μm/s)
0
.08
.16
.24
.32
.40
.48
.56
.64
V_G GROWTH VELOCITY (μm/s)

8.1

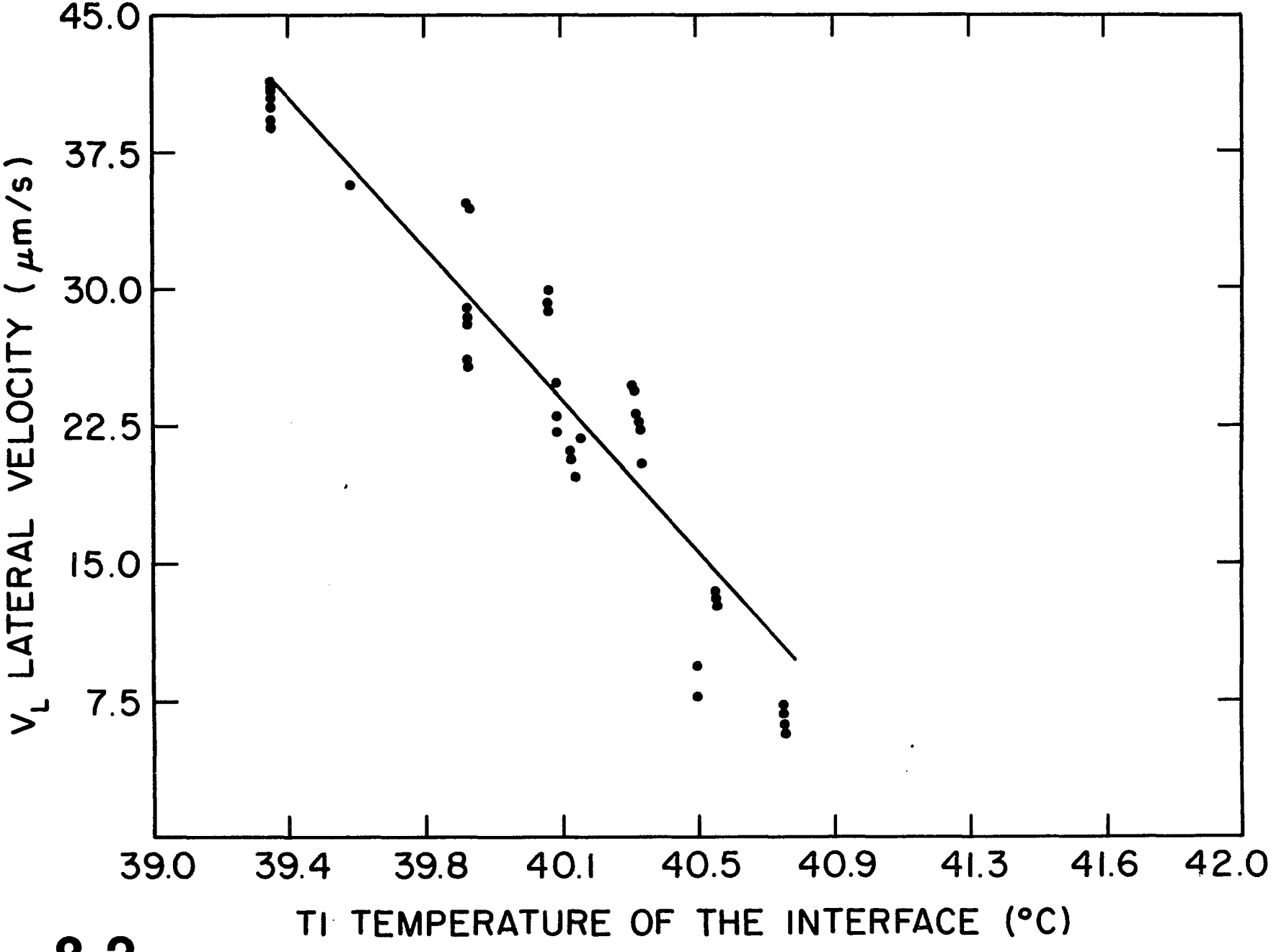
45.0
37.5
30.0
22.5
15.0
7.5
V_L LATERAL VELOCITY (μm/s)
39.0
39.4
39.8
40.1
40.5
40.9
41.3
41.6
42.0
TI TEMPERATURE OF THE INTERFACE (°C)

8.2